Green Chemistry

PAPER

Enhancing sustainable energy production through co-polyamide membranes for improved pressure-retarded osmosis performance and environmental impact: synthesis and life cycle analysis†

Cite this: DOI: 10.1039/d4gc03963g

Sadegh Aghapour Aktij,[a,b] Mostafa Dadashi Firouzjaei, *[b,c] Mohsen Pilevar,[c] Asad Asad Asad, [d] Ahmad Rahimpour,*[b] Mark Elliott,[c] João B. P. Soares*[a] and Mohtada Sadrzadeh *[b]

Received 9th August 2024,
Accepted 11th November 2024

DOI: 10.1039/d4gc03963g

rsc.li/greenchem

This study investigates the application of innovative co-polyamide (Co-PA) membranes in the pressure-retarded osmosis (PRO) process. The Co-PA membranes were synthesized *via* a polycondensation reaction of a mixture of *m*-phenylenediamine (MPD) and piperazine (PIP) with trimesoyl chloride (TMC). Characterization using attenuated total reflectance-Fourier transform infrared (ATR-FTIR) and X-ray photoelectron spectroscopy (XPS) confirmed chemical modifications in the membranes, while Atomic Force Microscopy (AFM) demonstrated increased surface roughness with PIP incorporation. Results showed that incorporating 1.5 wt% PIP significantly improved PRO performance, achieving a remarkable power density of 10.22 W m^{-2} and a 41.5% increase in water flux compared to the pristine TFC membrane. Additionally, XPS analysis demonstrated an increase in the degree of crosslinking, reducing reverse salt flux by 36.7%. A life cycle assessment of PRO systems was conducted to evaluate the environmental impact of the technology with developed membranes. The results confirm the environmental benefits of this novel membrane synthesis approach, indicating a reduction in cumulative energy demand (CED) and a shift towards more sustainable energy sources. This research highlights the potential of Co-PA membranes to revolutionize PRO technology, offering sustainable solutions for energy generation and water treatment. The findings contribute valuable insights into the environmental implications of PRO, which are essential for developing sustainable PRO systems.

1. Introduction

The demand for energy worldwide significantly outstrips the current production capabilities.[1,2] The predominant reliance on fossil fuels for energy is unsustainable, given their contributions to air pollution and greenhouse gas emissions.[3,4] Despite advancements in diversifying energy technologies, fossil fuel dependence persists in meeting global energy needs.[5,6] Processes that release Gibbs free energy during mixing offer significant potential for harnessing renewable energy. Technologies like reverse electrodialysis, capacitive mixing, and PRO exemplify effective means of capturing and utilizing this energy, playing a crucial role in diversifying and enhancing sustainable energy production.[7,8]

Pressure-Retarded Osmosis (PRO) is a technology that utilizes the osmotic pressure differential between solutions with different salt concentrations to produce electricity.[9] In this process, a semipermeable membrane is employed to separate a feed solution of lower concentration from a draw solution of higher concentration.[10] This separation creates an osmotic pressure gradient, compelling water to flow under pressure from the feed into the draw solution, where it drives a hydro turbine to generate electricity.[11] Despite notable technological advancements in PRO, its wider commercial application is hindered by the absence of membranes capable of achieving sufficiently high power densities.[12] Existing commercial nanofiltration (NF), reverse osmosis (RO), and forward osmosis (FO)

[a]Department of Chemical & Materials Engineering, Donadeo Innovation Centre for Engineering, Group of Applied Macromolecular Engineering, University of Alberta, Edmonton, AB T6G 1H9, Canada. E-mail: jsoares@ualberta.ca
[b]Department of Mechanical Engineering, Donadeo Innovation Center for Engineering, Advanced Water Research Lab (AWRL), University of Alberta, Edmonton, AB, T6G 1H9, Canada. E-mail: mdfirouzjaei@crimson.ua.edu, arahimpo@ualberta.ca, sadrzade@ualberta.ca
[c]Department of Civil, Construction, and Environmental Engineering, University of Alabama, Tuscaloosa, AL, 35487, USA
[d]Department of Mechanical Engineering, University of Alberta, Nanotechnology Research Centre, T6G 2M9, Canada

† Electronic supplementary information (ESI) available. See DOI: https://doi.org/10.1039/d4gc03963g

membranes exhibit suboptimal structural designs for PRO applications, leading to energy outputs substantially below the levels needed for efficient PRO operations. RO membranes, typically optimized for high salt rejection and low water permeability to effectively desalinate water, do not align with the needs of PRO, where higher water permeability and some degree of salt passage might be desirable to enhance osmotic flow and energy production.[13] Additionally, the structure of RO/NF membranes results in internal concentration polarization (ICP), hampering water flux.[14] Similarly, while the widely studied commercial FO membrane produced by Hydration Technology Innovations (HTI), the asymmetric cellulose triacetate-based membrane, outperforms RO/NF counterparts in PRO, it falls short of the economically viable power density threshold of 5 W m^{-2}.[13] Many developed FO membranes over the past decade have also been evaluated for PRO use, but these membranes often suffer deformation or damage under the high-pressure PRO.[13] Designed to be thin and porous to reduce ICP, FO membranes generally lack the mechanical strength necessary for effective use in PRO processes.[13]

Despite being the subject of research for several decades, the advancement of PRO beyond current power generation technologies has been hindered by the absence of efficient membranes, possessing high water permeability and solute selectivity.[15,16] Polyamide thin film composite (TFC) membranes, known for their high permselectivity, are widely used in PRO applications.[14,17] Polyamide TFC membranes are fabricated through interfacial polymerization (IP), a process involving the reaction of an amine from an aqueous phase with an acid chloride from an organic phase.[18–20] Amines typically used in this process include *m*-phenylenediamine (MPD), piperazine (PIP), and ethylenediamine (EDA), which are highly reactive with trimesoyl chloride (TMC).[21,22] Different molecular selections lead to the development of diverse PA structures critical for customizing TFC membranes.[23] Following the development of TFC membranes, significant research efforts have been dedicated to improving the physicochemical characteristics of the polyamide layer, focusing on increasing water permeance and solute rejection, to expand their range of applications.[24,25] This involves approaches such as monomer selection,[26,27] surface functionalization,[28–31] additive incorporation,[32,33] interlayer introduction,[34–36] *etc*. Despite considerable advancements in the development of hydrophilic,[37,38] chlorine-resistant,[39,40] and fouling-resistant[41–43] TFC membranes, progress in the fabrication of PRO TFC membranes for industrialization remains relatively modest. A critical approach in chemical modification involves constructing a membrane with a co-polyamide (Co-PA) active layer by integrating two distinct amine monomers during the IP process. Commonly, traditional RO membranes are fabricated by crosslinking an aromatic amine, such as MPD, with TMC. Conversely, an aliphatic amine like PIP is frequently employed in the fabrication of NF membranes. The innovation of Co-PA membranes has been an area of extensive research aimed at imbuing membranes with diverse physicochemical properties. For instance, a dual aromatic amine system comprising MPD and 3,5-diamino-*N*-(4-aminophenyl) benzamide (DABA) has demonstrated enhanced permeate flux attributed to DABA's additional carboxylic group.[44] Tang *et al.*[45] successfully produced a chlorine-resistant NF membrane by combining the aliphatic amine PIP with an aromatic amine, 2,2′-bis(1-hydroxyl-1-trifluoromethyl-2,2,2-trifluoroethyl)-4,4′-methylenedianiline, crosslinked with TMC on a polysulfone support layer. This NF membrane exhibited a high flux rate of 79.1 LMH and an impressive 99.5% rejection of Na_2SO_4. Similarly, Jin *et al.*[46] employed a blend of two aliphatic amines, tris(3-aminopropyl)amine and PIP, to create a high-performance, positively charged NF membrane, achieving a permeance of 10.2 LMH per bar and a 92.4% rejection of $MgCl_2$. These advancements demonstrate the significance of strategic amine selection in the IP reaction with TMC as a crosslinker, leading to membranes with superior salt rejection, increased permeate flux, and enhanced fouling resistance.[22] By integrating the characteristics of MPD-TMC and PIP-TMC, it is anticipated that a new network structure will be achieved with a novel combination of a PIP monomer with the MPD monomer in aqueous solution.[23,47]

A wide variety of amines featuring three or four active amine functions, combined with hexane-soluble cross-linkers such as TMC, enable enhanced control over the pore structure and thickness of the polyamide active layer. This control facilitates the fabrication of thin, selective, and densely cross-linked polyamide networks.[26] Wang *et al.*[48] successfully enhanced the water permeance of RO membranes by incorporating PIP into the MPD solution, achieving a water permeance three times higher than the unmodified membrane. Despite this significant increase in permeance, the addition of PIP resulted in a reduced NaCl rejection, declining from 99.0% to 95.0%. Yang *et al.*[49] described the development of a double-layered polyamide membrane, constructed through IP between PIP and TMC on MPD crosslinked PA substrate, achieving up to 99.13% NaCl and 97.45% Na_2SO_4 rejections, respectively, demonstrating its exceptional selectivity. In a study conducted by Cheng *et al.*,[50] TFC NF membranes were synthesized using PIP and MPD, achieving a high magnesium–lithium separation efficiency with a ratio of 28 in salt-lake brine. The application of these prepared NF membranes to magnesium–lithium separation yielded high rejection rates of 98.51% for magnesium ions and 96.01% for lithium ions, respectively, with a water flux of 30.4 LMH. Although considerable research efforts have focused on enhancing the performance and extending the application range of membranes fabricated from PIP and TMC for diverse scenarios,[47,49,51,52] the specific application and optimization of this mixture for PRO processes have yet to be explored. Therefore, this study demonstrates the fabrication of a novel customized TFC membrane with a Co-PA active layer for PRO. By combining PIP and MPD, we aim to design a membrane capable of achieving high power density in the PRO process. The membrane's performance was assessed in a PRO setup using synthetic brine as the draw solution and DI water as the feed solution. The observed enhancements in water flux, selectivity, and fouling resistance empha-

 This journal is © The Royal Society of Chemistry 2024

size the significant impact of our novel methodology, providing basic criteria for designing specialty PRO membranes for sustainable power generation. Moreover, research on the application of PA membranes in PRO has predominantly focused on synthesis processes, with limited insight into the associated energy demands and environmental impacts of these fabrication processes. Life cycle assessment offers a method for quantifying the overall efficiency of product fabrication.[53–56] This is particularly crucial in PRO, where energy production is a key factor, making it essential to evaluate the environmental and energy impacts of any modifications in product development. Therefore, this study pioneers an evaluation of the environmental impacts and energy requirements of membrane fabrication, providing a comprehensive assessment for potential scale-up.

2. Materials and methods

2.1. Materials and chemicals

All chemicals used in this study were used as received. Commercial polyethersulfone substrates with a pore size of 0.2 microns were purchased from Sterlitech Co. Piperazine (PIP, 99%), *m*-phenylenediamine (MPD, >99%), Camphorsulfonic acid, and trimesoyl chloride (TMC, 98%) were all obtained from Sigma-Aldrich. Triethylamine (TEA), sodium dodecyl sulfate (SDS), *n*-heptane, and sodium chloride (NaCl) were purchased from Fisher Scientific.

2.2. Polyamide membranes fabrication and characterization

To fabricate polyamide membranes, IP was performed on the surface of PES substrates.[57] The PES support was initially immersed in the MPD solution containing 0.5 wt% MPD, 0.2 wt% SDS, and 1.0 wt% TEA for 3 min. After removing the excess MPD solution using a roller, the TMC solution comprising 0.4 wt/v% TMC was poured on the membrane surface and kept for 60 seconds to allow the polymerization reaction to complete (referred to as pristine TFC membranes without PIP). The TFC-PIP membranes were fabricated using the same procedure, except PIP was added to the MPD solution at concentrations of 0.5, 1.0, 1.5, and 2.0 wt%. After forming the selective layer, the membranes were subjected to heat-curing in an oven at 60 °C for 4 minutes. The cured membranes were then stored in deionized water at 20 °C until testing was conducted. The modified membranes fabricated using PIP at concentrations of 0.5, 1.0, 1.5, and 2.0 wt% were designated as TFC-PIP0.5, TFC-PIP1, TFC-PIP1.5, and TFC-PIP2, respectively. Fig. 1 provides an overview of the fabrication process.

Field emission scanning electron microscopy (FESEM, JEOL FE 7000, JEOL, USA) equipped with an energy-dispersive X-ray (EDX) spectrometer at an accelerating voltage of 30 kV and transmission electron microscopy (TEM, Philips/FEI Morgagni 268, USA) were employed to analyze the surface and cross-sectional morphologies of the membranes. The chemical characteristics of the nanomaterials and the membranes were investigated with and attenuated total reflectance-Fourier transform infrared (ATR-FTIR) performed by an Agilent Technologies Cary 600 series FTIR spectrometer and X-ray photoelectron spectroscopy (XPS) using a Kratos AXIS ULTRA XPS. The absorbance spectrum of the membranes was quantified across a range from 400 to 4000 cm^{-1}, using a resolution of 4 cm^{-1}.[58] Surface roughness parameters were obtained by scanning a 10 μm × 10 μm area on each membrane, employing an atomic force microscope (AFM, model Bruker Dimension Icon, USA). The acquired data was subsequently analyzed using Gwyddion software, version 2.62. The root mean square (R_q) of the Z data and the mean roughness (R_a) were determined using the Nanoscope analysis software. The membranes' wettability was evaluated with a contact angle analyzer (DSA 100, KRÜSS, USA) equipped with image processing software. The contact angles provided are the mean values derived from measurements at five different points on three separate membrane samples. The zeta potential of the surfaces of the fabricated membranes was measured between a pH of 4 and 9 using a SurPASS Electrokinetic Analyzer (Anton Paar, Graz, Austria). A 1 mM KCl solution at 25 °C served as the electrolyte, while 0.05 M solutions of HCl and NaOH were used to modify the solution's pH. Each measurement was performed in triplicate to ensure the reliability and consistency of the results.

2.3. Evaluation of membrane performance

Membrane performance in osmotic separation was assessed using a cross-flow FO/PRO system at 25 ± 0.5 °C. The active surface area of the studied membrane was 20.6×10^{-4} m^2. The FO/PRO system can function in two configurations: with the active layer oriented towards the feed solution (AL-FS) and with the active layer directed towards the draw solution (AL-DS). The cross-flow velocity for both feed solution (FS) and draw solution (DS) streams was set to 1.5 L s^{-1}. For the FS and DS, deionized water and 0.5, 1, 1.5, and 2 M NaCl solutions were employed, respectively. The osmotic water flux (J_w) in the FO process was calculated as follows:[59,60]

$$J_w = -\frac{\Delta(m_{fs} \cdot y_w)}{\Delta t} \frac{1}{\rho_w A_m} \quad (1)$$

where m_{fs} represents the mass of the feed solution in the tank, ρ_w denotes the density of pure water, y_w is the water's mass fraction in the feed solution in the tank, and A_m denotes the membrane area. The change in (m_{fs}·y_w) over the time interval Δt is denoted as $\Delta(m_{fs}$·$y_w)$. In the FO process, the reverse salt flux was calculated using the following equation:[59,60]

$$J_s = -\frac{\Delta(m_{fs} \cdot y_s)}{\Delta t} \frac{1}{\rho_s A_m} \quad (2)$$

In this equation, y_s represents the mass fraction of NaCl in the FS within the tank and ρ_s is the NaCl density. The water flux (J_w) and reverse salt flux (J_s) of the prepared membranes in the PRO process were determined by applying eqn (1) and (2) with a deionized water as feed solution and a 1.0 M NaCl as draw solution. After membrane pre-compaction at 10 bar for 2 h, J_w and J_s were evaluated by increasing the transmembrane

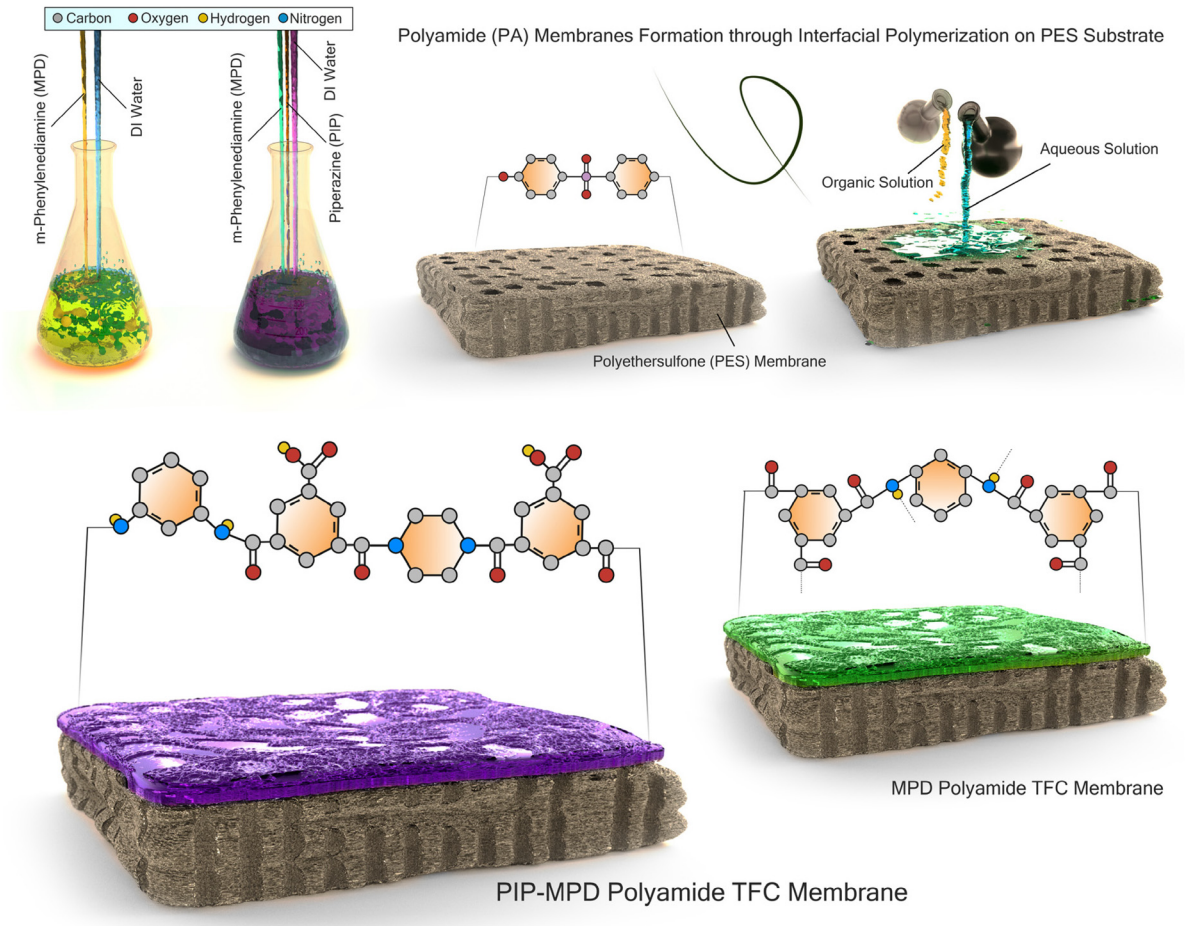

Fig. 1 The schematic representation delineates the fabrication process of both TFC and TFC-PIP membranes, highlighting the synthesis of a novel network structure achieved through the innovative combination of PIP and MPD monomers in an aqueous solution. This method is strategically directed towards refining the properties of polyamide membranes to broaden their applications, particularly in enhancing power generation through PRO. Ensuring a defect-free membrane structure in the fabrication process necessitates meticulous surface conditioning and interface management, emphasizing the critical importance of selecting suitable materials and maintaining structural integrity. The diagram summarizes the project's objectives: to optimize PIP concentrations for effective separation and to enhance membrane performance characteristics, such as permeability, selectivity, and power generation capability. This figure exemplifies the intricate equilibrium between material selection and composition optimization, fundamental in the realm of advanced separation technologies.

pressure (ΔP) from 0 to 8 bar using a bench-scale PRO setup (Fig. 2). Detailed information about this setup is provided in ESI (S1).† For energy production, the power density of the membrane (W m^{-2}) was determined using the following equation:[61–63]

$$W = J_w \cdot \Delta P \quad (3)$$

2.4. Life cycle assessment

The LCA was applied to analyze the environmental impacts of generating electricity using the synthesized PRO membranes. This analysis focused on a particular area in Alberta, Canada, and considered every stage of the membrane's life cycle, from production to use and disposal, as shown in Fig. 3. Membrane areas were calculated based on power densities to meet the energy requirements. The study adhered to ISO 14040/14044 standards, employing the ReCiPe midpoint method within the OpenLCA framework and ecoinvent database for assessing impact categories like global warming potential. Sensitivity and uncertainty analyses addressed variabilities and assumptions within the LCA model. Comparative LCA was executed between laboratory-scale and potential industrial-scale (roll-to-roll manufacturing) membrane units, focusing on material and energy consumption, detailed in the ESI (S2).† A life cycle impact assessment was conducted to determine the Cumulative Energy Demand (CED), and the Tool for the Reduction and Assessment of Chemical and other Environmental Impacts (TRACI 2.1) was used to ascertain the environmental impacts. The selection of impact categories was guided by the US EPA's taxonomy analysis, considering the holistic implications of environmental impacts. Detailed LCA methodologies, definitions of impact categories, and a complete inventory list of calculations can be found in the ESI (S2).† The surface areas required for each membrane type, the

 This journal is © The Royal Society of Chemistry 2024

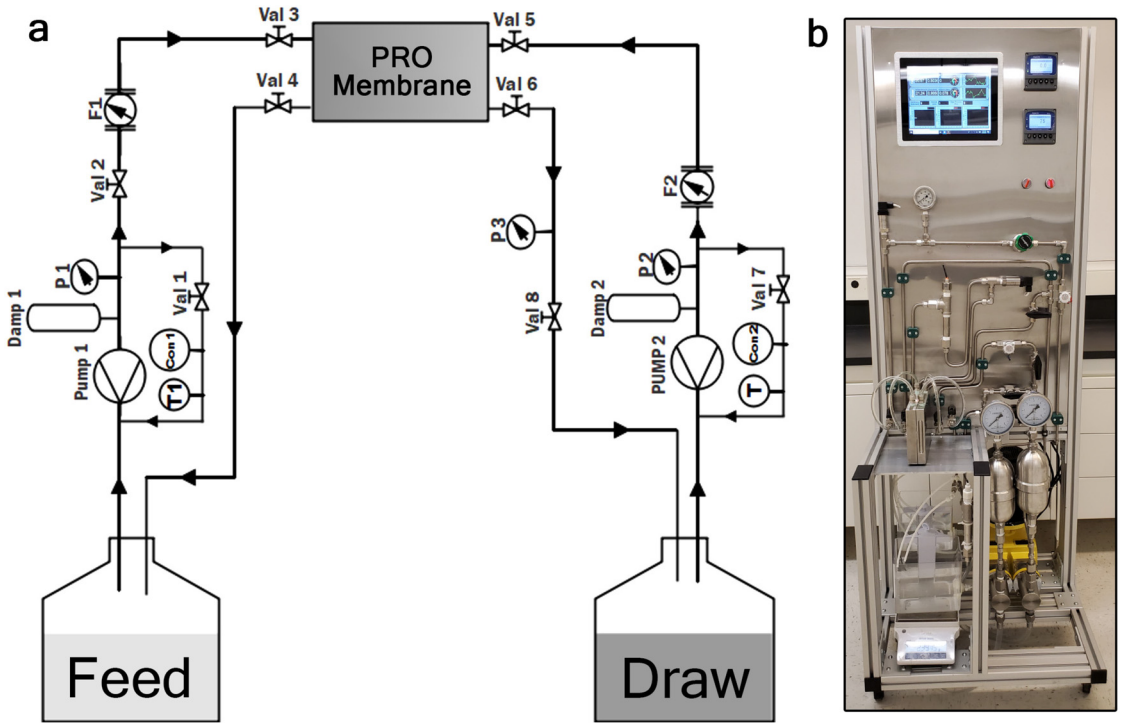

Fig. 2 Schematic flow diagram (a) and picture (b) of the laboratory PRO experimental setup.

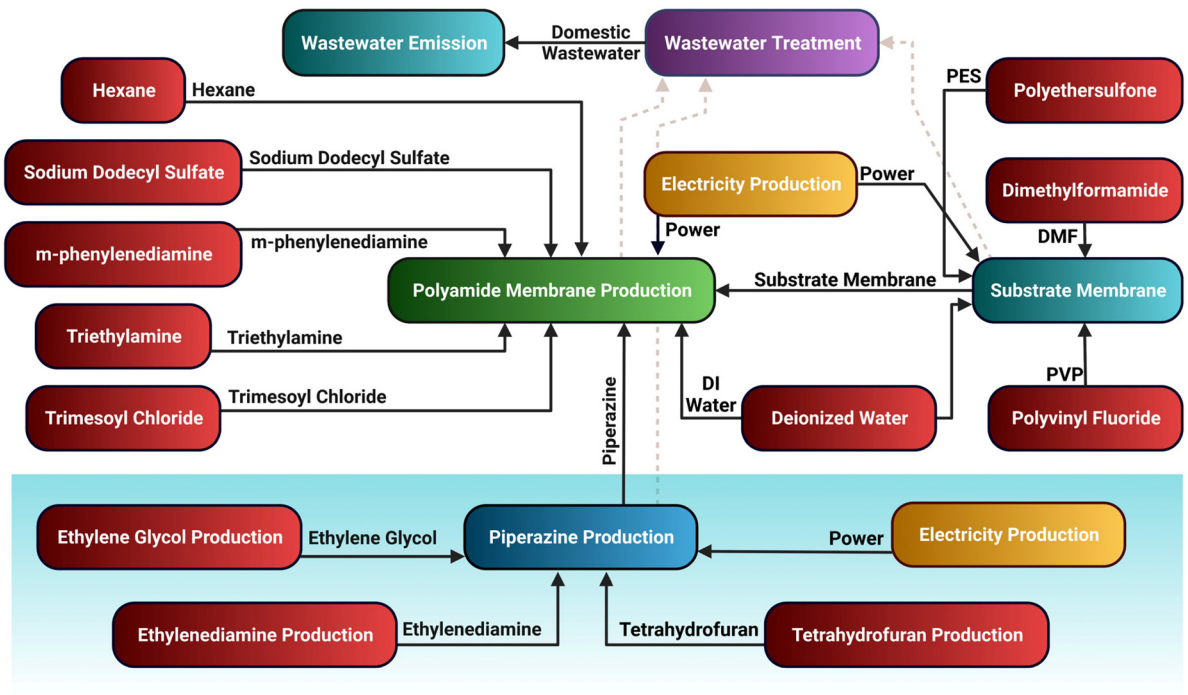

Fig. 3 The conceptual synthesis schematic of PRO TFC membranes. The flow diagram illustrates the interconnected procedures in manufacturing polyamide membranes, emphasizing the materials and results at each step. The scheme begins by acquiring raw materials and then follows the process of synthesizing important intermediates, such as piperazine. This process ultimately leads to the production of the polyamide membrane. The diagram depicts the energy inputs needed for the synthesis processes and the wastewater treatment that is necessary to address emissions from the system.

Table 1 The surface area needed for each membrane based on their power density to generate electricity for 10 days for 2000 individuals in Alberta, Canada

Membrane	Power density (W m^{-2})	Surface area (m^2)
TFC	5.33	390 0697.49
TFC-PIP0.5	7.33	284 103.22
TFC-PIP1	8.44	246 681.74
TFC-PIP1.5	10.22	203 787.24
TFC-PIP2	10.00	208 333.30

key to fulfilling the LCA's functional unit, are summarized in Table 1, with extensive calculations documented in the accompanying Excel file, available in the ESI.†

3. Results and discussion

3.1. Surface characteristics of the membranes

ATR-FTIR spectroscopy was utilized to analyze the surface chemistry of both pristine TFC and TFC-PIP membranes, as demonstrated in Fig. 4a. The observed peak at 1485 cm^{-1} indicates the C–C stretching vibrations within the aromatic rings.[64,65] Additionally, the peaks observed at 1300 and 1321 $cm^{-1}$are associated with the stretching vibrations of the O═S═O group.[32,64] Peaks appearing at 1144 and 1245 cm^{-1}can be ascribed to the phenyl ring and the asymmetric C–O–C group within the PES substrate, respectively.[59] In the spectral analysis of the TFC membrane, the PA layer's distinctive peaks are apparent at 1541 cm^{-1} (amide II, coupled C–N and N–H bending stretching vibration of a –CO–NH– group[66]), 1611cm^{-1} (N–H of amide[67]), and 1660 cm^{-1}(amide I, stretching vibration of C═O[57]). For TFC-PIP membranes, a distinctive peak is observed at 1630 cm^{-1}. This peak, positioned distinctly between the 1611 cm^{-1} (attributed to N–H of amide) and 1660 cm^{-1} (associated with amide I, stretching vibration of C═O) peaks, not only supersedes these two peaks but also alters their intensities. The 1630 cm^{-1} peak, the C═O stretching (carbonyl in amide I), serves as a definitive signature of poly(piperazinamide) linkages present within the selective layers of all TFC-PIP membranes.[68,69] Furthermore, the absorption peaks of C–N/N–H at 1541 cm^{-1} in TFC-PIP membranes were comparatively weaker than pristine TFC due to the formation of tertiary amide (–CONR) through crosslinking between PIP and TMC, resulting in less amidic hydrogen.[70] Alterations in peak intensities, coupled with the emergence of a new peak, signify the formation of Co-PA, including both fully aromatic polyamide (derived from MPD and TMC) and semi-aromatic poly(piperazine-amide) (originating from PIP and TMC). The hypothetical IP reaction scheme between mixed MPD/PIP and TMC, along with the potential structure of the resulting mixed polyamide network as suggested by FTIR and XPS analyses, is depicted in Fig. 1S.†

The XPS survey spectra of TFC and TFC-PIP membranes in Fig. 4b reveal the existence of three primary elements: carbon, oxygen, and nitrogen, positioned approximately at 285, 532,

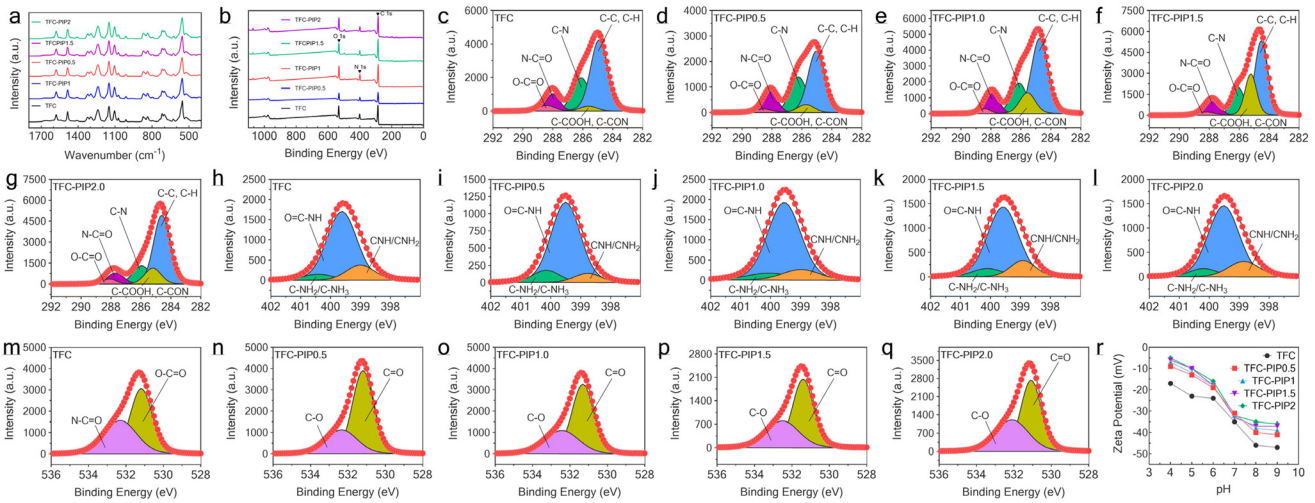

Fig. 4 (a) ATR-FTIR spectra of TFC and TFC-PIP membranes, highlighting semi-aromatic poly(piperazinamide), fully aromatic polyamide, and PES substrate peaks. In TFC-PIP membranes, alterations in peak intensities, coupled with the emergence of a new peak at 1630 cm^{-1}, signifying the formation of both fully aromatic polyamide (derived from MPD and TMC) and semi-aromatic poly(piperazinamide) (originating from PIP and TMC), distinguishing it from the TFC membrane, which only contains fully aromatic polyamide. (b) Proposed structure of the resulting mixed polyamide network formed by combining *m*-phenylenediamine (MPD) and piperazine (PIP) as monomers. (b–r) XPS survey spectra of the TFC and TFC-PIP membranes. (b) General survey XPS spectra of the TFC and TFC-PIP membranes. (c–q) Deconvoluted high-resolution XPS spectra; C 1s, N 1s, and O 1s for the TFC and TFC-PIP membranes. During the polymerization reaction, an increase in the formation of amide linkages and a decrease in the hydrolysis of acyl chloride groups lead to a higher proportion of N–C═O to O–C═O. This results in a lower O/N ratio and a higher degree of crosslinking in the polyamide layer. (r) Zeta potential analysis from pH 4 to 9 reveals a more negative surface charge on TFC membranes relative to TFC-PIP membranes. This difference is attributed to the nitrogen-containing groups in PIP, which impart positive charges and slightly reduce the negative charge on the membrane surface.

This journal is © The Royal Society of Chemistry 2024

Table 2 Comparative elemental compositions and key peak characteristics of TFC and TFC-PIP membranes as determined by XPS analysis

Membrane	Carbon	Oxygen	Nitrogen	O/N ratio	Cross-linking degree	C–C, C–H	C–COO, C–CON	–CN–	N–C=O	O–C=O	$\frac{N-C=O}{O-C=O}$
TFC	74.88	15.75	9.37	1.25	67	55.36	3.85	25.78	10.63	4.37	2.43
TFC-PIP0.5	73.64	15.34	11.02	1.08	89	48.81	6.46	28.30	13.63	2.86	4.76
TFC-PIP1	74.33	14.76	10.92	1.11	84	50.88	12.03	20.95	13.04	3.10	4.21
TFC-PIP1.5	77.80	13.34	8.86	1.15	79	44.10	22.89	17.30	12.49	3.21	3.89
TFC-PIP2	74.81	16.42	8.77	1.18	76	55.35	13.39	16.32	11.64	3.30	3.53

and 399 eV 30, respectively. Table 2 presents the elemental compositions and notable peak attributes of the TFC and TFC-PIP membranes, as determined from the XPS analysis. The high-resolution C 1s and N 1s spectra are deconvoluted to five and three peaks, respectively, as depicted in Fig. 4c–g and h–l. The peak at 285 eV is due to C–C/C–H bonds present in the cyclic structures of hydrocarbon chains of the membrane.[71] The peaks at 285.7 eV can be attributed to carbon attached to the carboxyl (C–COOH) and amine linkage (C–CON).[72] The peak at 286.2 eV can be assigned to the –CN– bond, possibly resulting from the carbon attached to an amide linkage or from unreacted amines.[26] The peaks at 288.1 eV and 288.6 are due to the presence of N–C=O (amide linkage) and O–C=O (carboxyl group) in the membrane, respectively.[73] The N 1s XPS data of the TFC and TFC-PIP membranes exhibits a broad peak centered around 401 eV. The peak can be deconvoluted into three distinct components at 398.1 eV, 399.9 eV, and 400.2 eV, each representing the unique chemical environments of the nitrogen atoms within the membrane. Specifically, the peak at 398.1 eV is indicative of the CNH/CNH_2 group, while the peak at 399.9 eV is associated with the O=C–NH group, confirming the successful formation of the selective layer.[47,71,74,75] Furthermore, the peak at 400.2 eV is likely representative of the C–NH^{2+}/C–NH^{3+} group. The high-resolution O (1s) spectra for both TFC and TFC-PIP membranes reveal two distinct peaks at approximately 531.6 and 533.0 eV, as depicted in Fig. 4o–q. These peaks correspond to the C=O group, which includes the amide bond (N–C=O) and the carboxyl group (O–C=O), and to the C–O group found in carboxylic acid moieties, respectively.[76,77] This carboxylic acid group, typically found on the surface of polyamide membranes, can emerge from the hydrolysis of unreacted acyl chlorides.[78] We also calculated the oxygen to nitrogen (O/N) ratio of the prepared membranes to provide an insight into the crosslinking degree of the polyamide layer; the fully cross-linked structure, theoretically, has an O/N ratio of 1.00.[72] Table 2 reveals that the O/N ratio of the TFC-PIP membranes was consistently lower than that of the TFC membrane (without PIP), indicating a higher cross-linking degree. From the high-resolution O (1s) spectra presented in Fig. 4o–q, it can be observed that the oxygen in the PA layer predominantly originates from the amide bond (N–C=O) at 531.6 eV, which results from the crosslinking reaction between the amine and acyl chloride, along with the carboxyl (O–C=O) at 533.0 eV, which was formed through the hydrolysis of acyl chloride.[79] Therefore, during the polymerization reaction, an increase in the formation of amide linkages and a decrease in the hydrolysis of acyl chloride groups lead to a higher proportion of N–C=O to O–C=O. This results in a lower O/N ratio and a higher degree of crosslinking in the polyamide layer. For instance, the O/N ratio of polyamide layers declined from 1.25 in TFC membrane (without PIP) to 1.08 in TFC-PIP0.5. Simultaneously, the N–C=O to O–C=O content increased from 2.43 to 4.76. This was accompanied by an increase in the degree of crosslinking, going from 67% to 89%. The increase of the crosslinking degree observed upon the addition of PIP is primarily attributed to the increased accessibility of the diamine monomer, which facilitates the formation of a more cross-linked selective layer,[80] as illustrated in the molecular structures of developed membranes (Fig. 1S†). Additionally, introducing PIP elevates the alkalinity of the aqueous solution. This enhances the amine solution's ability to neutralize the hydrochloric acid formed during the amine and acyl chloride reaction, thereby the polymerization was promoted toward a higher extent.[81] However, as the concentration of PIP increased, the O/N ratio showed an upward trend, suggesting that the active layer of the resultant membrane had a decreasing degree of cross-linking with the increase in PIP concentration. Since the MPD and PIP are cross-linked by TMC molecules during the polymerization process, a high concentration of amine monomers possibly led to a deficit in TMC,[82] leading to a polyamide layer with lower cross-linking density. This, in turn, likely resulted in increased water permeability and reduced salt rejection.[81]

The zeta potential of the fabricated membranes, assessed across a pH range of 4 to 9 using the streaming potential method, is displayed in Fig. 4r. Over this pH range, every membrane displayed a negative surface charge. This charge behavior can be linked to the protonation and deprotonation of functional groups within the polyamide structure of the TFC and TFC-PIP membranes.[83] Typically, at low pH, the protonation of amine groups (–NH_2) into R-NH_3^+ imparts a positive charge to the membrane, whereas at high pH, the deprotonation of carboxylic acid groups (–COOH) into R-COO^- results in a more negatively charged surface.[84,85] The pH of the solution influences the degree of ionization and the membrane surface charge through the equilibrium dissociation reaction of R-COOH (R-COOH ⇔ R-COO^- + H^+) and R-NH_2 (R-NH_3^+ ⇔ R-NH_2 + H^+).[86] Incorporating PIP molecules increased the zeta potential of the TFC-PIP membranes, which was found to be dependent on PIP concentration. This phenomenon is attributed to the reaction between PIP and the acyl chloride of TMC monomers, resulting in a reduction of unreacted acyl chlorides

that would otherwise hydrolyze into carboxyl groups. This reaction renders the TFC-PIP membrane surface less negatively charged.[87,88] Moreover, the TFC-MPD membrane exhibited the highest absolute value of the zeta potential, indicative of the largest surface charge density,[89] consistent with XPS analysis results.[50] The presence of nitrogen-containing groups from PIP in the TFC-PIP contributed to an enhanced positive surface charge.[81,88] In addition to the above, it's also worth noting that the surface negative charges are typically influenced by the density of carboxylic groups present per unit of surface area.[90] At low PIP concentrations (TFC-PIP0.5), there is an initial reduction in the carboxylic group density, as indicated by the O–C═O content in the XPS data. This reduction in carboxylic groups results in a less negative surface charge. As the PIP concentration increases, the O–C═O content gradually rises; however, the accompanying increase in surface roughness (R_a), as shown by AFM data, causes these carboxylic groups to be distributed over a larger surface area. This expansion effectively lowers the local density of carboxylic groups per unit area, despite their overall increase in number. This reduction in carboxylic group density influences the zeta potential, potentially leading to a progressively less negative charge, as observed across the membranes from TFC-PIP0.5 to TFC-PIP2.[91]

The fabricated membranes' surface roughness was analyzed using AFM. Fig. 5a and b illustrate 3D and 2D AFM images, respectively, highlighting the surface morphology of the TFC and TFC-PIP membranes. These figures also provide the average roughness (R_a) and root-mean-squared roughness (R_q) values as indicators of the roughness parameters. The average roughness (R_a) of the TFC membrane is 152 nm, while the TFC-PIP membranes show a much rougher surface, with R_a ranging from 198 to 328 nm. These variations are likely due to the nature of the polymerization reaction. In the case of the TFC membrane (MPD/TMC), the amine groups are uniformly distributed along the polymer chains, resulting in a smoother interfacially polymerized surface layer.[87] However, when the amine reactants include a mixture of PIP and MPD, the local reaction rate between the amines and TMC varies, reflecting the differing reactivities and mobilities of the amine molecules.[87] The reduced polymerization rate of the aromatic monomer MPD with TMC, compared to the alicyclic monomer

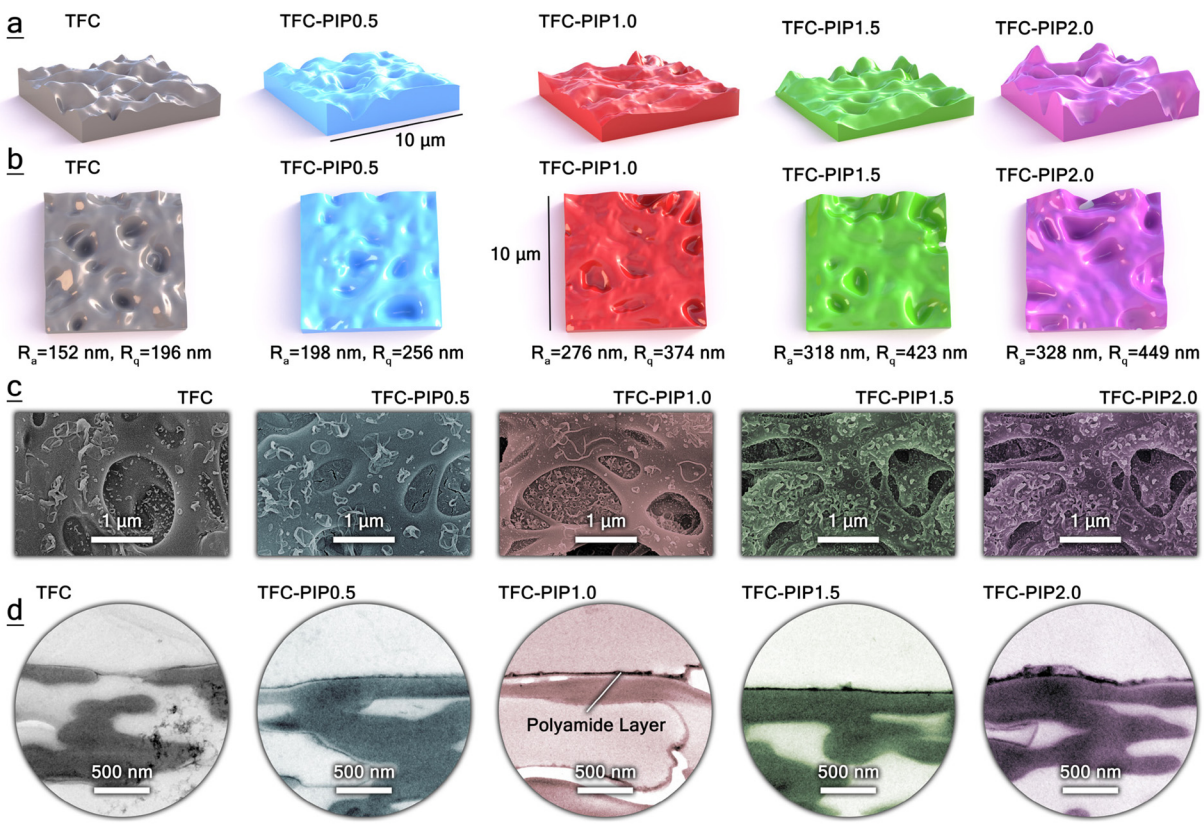

Fig. 5 (a) 3D and 2D (b) AFM images presenting the surface morphology of TFC and TTC-PIP membranes, along with R_a (average roughness) and R_q (root mean square roughness) parameters. Incorporating PIP molecules in TFC membranes increases surface roughness, which may correlate with enhanced water permeability and overall membrane performance in PRO application. (c) Top surface FE-SEM and (d) cross-sectional TEM images of TFC and TFC-PIP membranes. The images demonstrate that adding PIP affects the surface texture of the polyamide layer, making it grainier and rougher, particularly in TFC-PIP1.5 and TFC-PIP2 membranes. TEM analysis indicates that the polyamide layers in TFC-PIP membranes are thicker than those in TFC membranes, with the thickness increasing as PIP concentration rises. This change in thickness and texture may be due to PIP influencing the IP reaction's kinetics.

This journal is © The Royal Society of Chemistry 2024

PIP, may be due to MPD's larger molecular size and diminished chain mobility.[92] This difference likely leads to less pronounced nodule growth on the surface. Furthermore, PIP, a saturated heterocyclic amine characterized by its incorporation of nitrogen atoms within a six-membered ring structure, exhibits enhanced basicity. This structural arrangement facilitates greater accessibility of electron pairs on the nitrogen atoms, rendering PIP a notably potent base. Conversely, MPD, classified as an aromatic amine, features two amino groups linked to a benzene ring.[93–95] This aromatic configuration leads to the delocalization of nitrogen's lone pair electrons, diminishing their readiness for protonation and, thereby, reducing its basicity.[96] Consequently, PIP, with its more readily available nitrogen electron pairs, is generally more basic than MPD. This increased basicity of PIP augments the nucleophilicity of amine groups, which in turn heightens their reactivity towards electrophilic agents such as TMC in polyamide formation. This enhanced reactivity facilitates the IP reaction, favorably impacting the thermodynamics by rendering the free energy change more negative and thus, indicating a more favorable reaction.[97,98] With a higher PIP content in the amine mixture, the formation of PIP-TMC bonds occurs more rapidly, markedly influencing the slower crosslinking process between TMC and the amine groups in MPD.[87,88] This leads to rough surfaces with prominent ridge-valley patterns and even aggregated nodular structures. The rise in surface roughness could lead to a larger effective surface area for TFC-PIP membranes and promote a high surface hydrophilicity, which was seen as advantageous for improving the membrane's water permeability.[99]

The hydrophilicity of the membrane surface is crucial as it influences water permeability and antifouling properties. Water contact angle measurements, depicted in Fig. 2S,† were used to evaluate surface wettability. Compared to the water contact angle of 78° observed for the TFC membrane, the TFC-PIP membranes displayed lower water contact angles, indicating improved hydrophilicity of the modified membranes. As the concentration of PIP increased, the contact angle of the interfacially polymerized layer decreased from 68° for TFC-PIP0.5 to 53° for TFC-PIP2. This phenomenon can be attributed to the inherent properties of PIP, characterized by its heterocyclic amine structure with two nitrogen atoms and the absence of an aromatic benzene ring.[92] PIP's structure increases hydrophilicity, as the nitrogen atoms facilitate hydrogen bond formation, thus increasing the membrane's polarity.[47,100] In contrast, MPD is an aromatic diamine that presents a balance between hydrophobic and hydrophilic properties due to its benzene ring and amine groups.[92] Additionally, the surface physical heterogeneity, exemplified by surface roughness in alignment with the Wenzel[101] model, contributes to its more hydrophilic behavior.[86,102]

The surface morphology of TFC and TFC-PIP membranes was examined by FE-SEM, as illustrated in Fig. 5c. All membranes showed a distinct ridge and valley structure. As can be observed, the presence of PIP altered the surface texture to a nodular structure with more surface unevenness due to higher cross-linking that occurs during IP redaction. TEM cross-sectional images (Fig. 5d) confirmed the formation of a continuous polyamide layer over the porous support, providing clear evidence of polyamide formation with thicknesses below 100 nm. As observed, the polyamide layer thickness in the TFC-PIP membranes is higher than that in the TFC membrane, a difference that amplifies slightly with increasing PIP concentration. This phenomenon is likely due to the PIP's impact on the kinetics of the IP reaction.[103] Specifically, higher PIP concentrations enhance the amine monomer partition rate from water to *n*-heptane, thereby facilitating the growth of the polyamide layer.[104] Furthermore, the molar mass of PIP is 86.14 g mol^{-1}, marginally lower than that of MPD, which is 108.14 g mol^{-1}. This indicates that PIP may diffuse into the reaction zone more readily, owing to its lower molar mass.[92] Another critical aspect to consider is steric hindrance. MPD, characterized by its aromatic ring, exhibits greater steric hindrance compared to PIP, which possesses an alicyclic structure.[93,94] Consequently, the polyamide active layer synthesized from MPD and TMC—both featuring aromatic structures—demonstrates a more rigid polymer chain. The increased steric hindrance of MPD poses a challenge for its penetration through the active layer during the IP process.[87] As a result, the growth of the active layer is more rapidly restricted in the presence of MPD than with the PIP-TMC reaction, leading to the formation of a thinner and smoother active layer structure.

3.2. Membranes' osmotic filtrations performance

Fig. 6 presents the FO filtration performance of the TFC and TFC-PIP membranes at different PIP concentrations, tested in two distinct modes of AL-FS and AL-DS. The water flux (J_w), reverse salt flux (J_s), and the ratio of salt rejection to water flux (J_s/J_w) were evaluated. The increase in flux by raising the draw solution concentration is primarily attributed to the enhanced osmotic driving force. Nevertheless, when the NaCl concentration reaches higher levels, the flux demonstrates a nonlinear rise with a diminished slope, attributed to the accumulation of NaCl ions within the membrane support layer when operating in AL-FS mode, resulting in internal concentration polarization.[105,106] Conversely, in AL-DS mode, the polyamide layer experiences significant external concentration polarization (ECP) owing to the high salt concentration of the draw solution.[57,107] In both configurations, increasing the draw solution concentration enhances the accumulation of salt ions in the vicinity of the polyamide active layer, thereby reducing the effective osmotic pressure gradient across the membranes.[108] Additionally, it is noteworthy that the flux is higher in the AL-FS mode than in the AL-DS mode, indicating the more significant impact of ICP on the effective osmotic driving force than ECP. The results demonstrate an enhanced performance of TFC-PIP membranes compared to control TFC membranes, with improvements noted in both water flux and reverse salt flux (J_s). The incorporation of PIP into the selective layer plays a pivotal role in enhancing membrane performance by altering its physicochemical properties. As detailed in

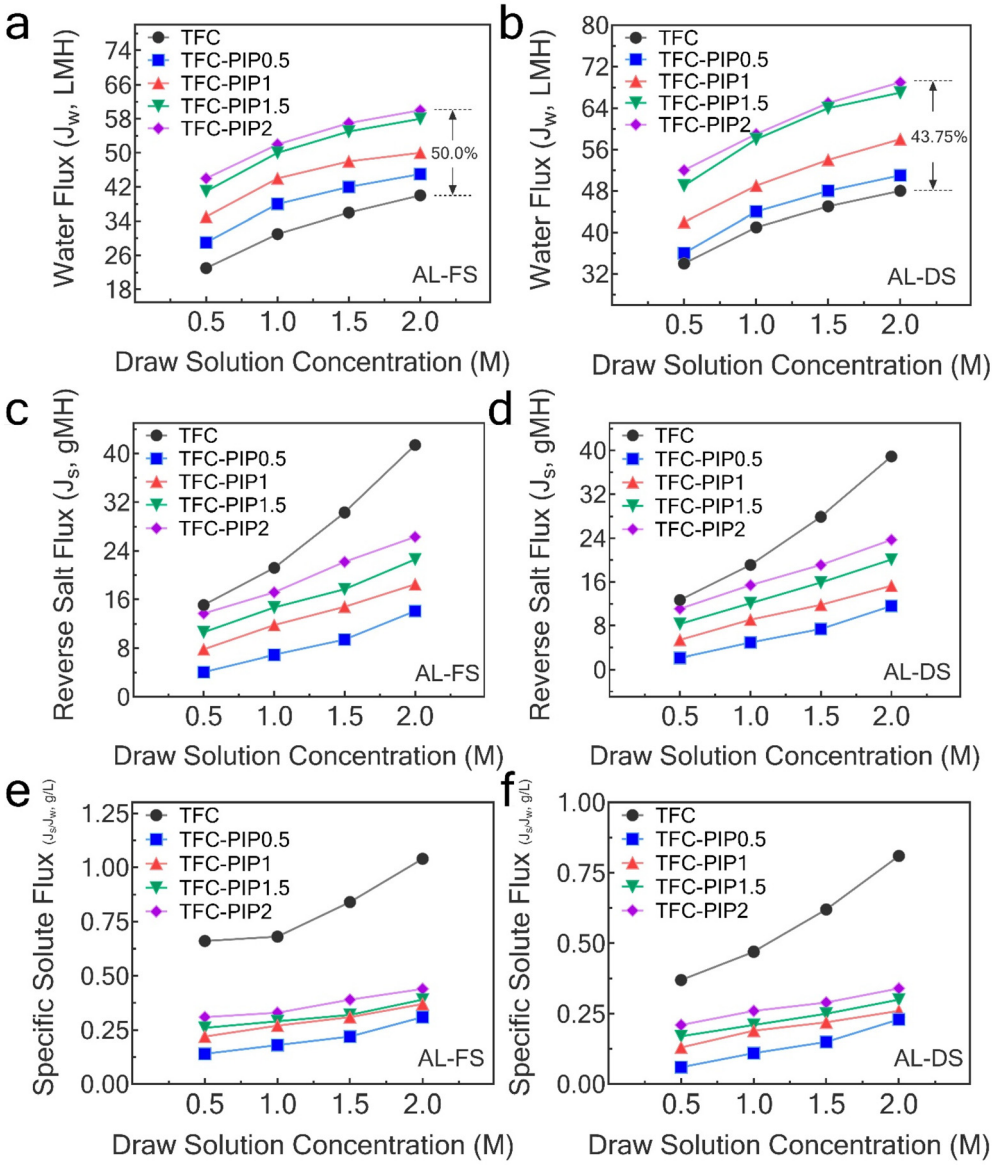

Fig. 6 (a) Water flux, (b) reverse salt flux, (c) specific solute flux in FO mode, (d) water flux, (e) reverse salt flux, (f) specific solute flux in PRO mode for TFC and TFC-PIP membranes with varying concentrations (0.5, 1, 1.5 and 2 wt%) of PIP. Filtration results demonstrate an enhanced performance of TFC-PIP membranes compared to control TFC membranes, with improvements noted in both water flux and reverse salt flux (J_s), in both FO and PRO modes. TFC-PIP1.5 exhibited nearly identical water flux as the TFC-PIP2 membrane, yet with a superior J_s/J_w ratio, indicating that it offers a higher separation efficiency than the other membranes.

section 3.1, a possible reason for the improved water flux is the enhanced surface hydrophilicity and roughness with the incorporation of PIP into the polyamide network. Additionally, the enhanced selectivity is likely due to the higher degree of cross-linking within the polyamide network, as confirmed by XPS analysis.

In the AL-DS mode with a 1 M draw solution, the TFC-PIP2 membrane exhibited the highest water flux of 59 LMH, which is 44% higher than the TFC membrane. Conversely, the TFC-PIP0.5 membrane exhibited the lowest reverse salt flux of 4.9 gMH, representing an improvement of approximately 74% compared to the TFC membrane. The specific solute flux (J_s/J_w) is a crucial performance metric for evaluating TFC membranes.[109] A lower J_s/J_w ratio is highly desirable, as it indicates enhanced selectivity and improved overall membrane productivity, allowing for greater water flux while minimizing salt passage. Fig. 6 illustrates that the TFC-PIP1.5 membrane has a J_s/J_w ratio of 0.21, coupled with a superior level of water transport.

Given that the power density of the PRO process is directly related to J_w, the monomer composition for TFC-PIP was optimized to increase J_w even though this involves a trade-off with J_s/J_w, which is particularly desirable for maximizing power density in an open-loop PRO process.[63,110] As a result, despite

 This journal is © The Royal Society of Chemistry 2024

the relatively lower selectivity (high J_s/J_w), significantly higher J_w was attained with the higher concentrations of PIP monomers. Notably, an increase in the PIP concentration from 5.0 to 1.5 wt% resulted in an enhanced J_w for the TFC-PIP1.5 membrane. From the results, it can be inferred that the TFC-PIP1.5 membrane showed a superior separation performance compared to the other membranes in AL-DS mode. Likewise, in the AL-FS mode with a 1 M NaCl draw solution, the TFC-PIP1.5 and TFC-PIP2 membranes significantly enhanced water flux values, reaching 50 LMH and 52 LMH, respectively. This represents an increase of approximately 61% and 68% compared to the TFC membrane. Moreover, there was a notable reduction in reverse salt flux, from 21.2 gMH in the TFC membrane to 14.7 gMH and 17.2 gMH for the TFC-PIP1.5 and TFC-PIP2 membranes, respectively. XPS analysis confirmed that the crosslinking degree increased with PIP concentration up to 1.5 wt%, but further increases (*e.g.*, TFC-PIP2) resulted in a lower crosslinking density due to excessive incorporation of PIP. This reduced crosslinking led to a slight decline in salt rejection efficiency, contributing to higher J_s values at higher PIP concentration. Thus, beyond the optimal concentration of 1.5 wt%, further increases in PIP begin to compromise membrane selectivity, even though water flux continues to rise marginally.

3.3. Membranes' power generation performance

Fig. 7 illustrates the PRO behavior of both TFC and TC-PIP membranes, evaluated with the system shown in Fig. 2 at a temperature of 25 °C and a pressure ranging from 0 to 10 ± 0.1 bar. Since the membranes' burst pressure falls between 8 and 9 bar, the assessment of power density was limited to a maximum hydraulic pressure of 8 bar. As depicted in Fig. 7a, the water flux (J_w) increased for both TFC and TFC-PIP membranes by increasing the pressure. Specifically, under an applied pressure of 8 bar, the incorporation of PIP led to a notable increase of about 92% and 88% in water flux for TFC-PIP1.5 and TFC-PIP2 membranes, respectively, in contrast to the pristine TFC membrane. Fig. 7b shows the PIP-containing membranes also excel in selectivity as they provide lower reverse salt flux (J_s).

As can be observed in Fig. 7c, the solute-to-water flux ratios (J_s/J_w) for all TFC-PIP1.5 and TFC-PIP2 membranes were found to be almost 66% and 62% lower than that of the TFC membrane at 8 bar. The TFC-PIP1.5 membrane exhibited a lower J_s/J_w ratio than TFC-PIP2, attributed to its enhanced water flux and reduced reverse salt flux. These findings suggest that the TFC-PIP1.5 membrane offers optimal performance in terms of higher flux during the PRO process without compromising membrane selectivity. Fig. 7d shows the relationship between experimental power density and the pressure gradient for both

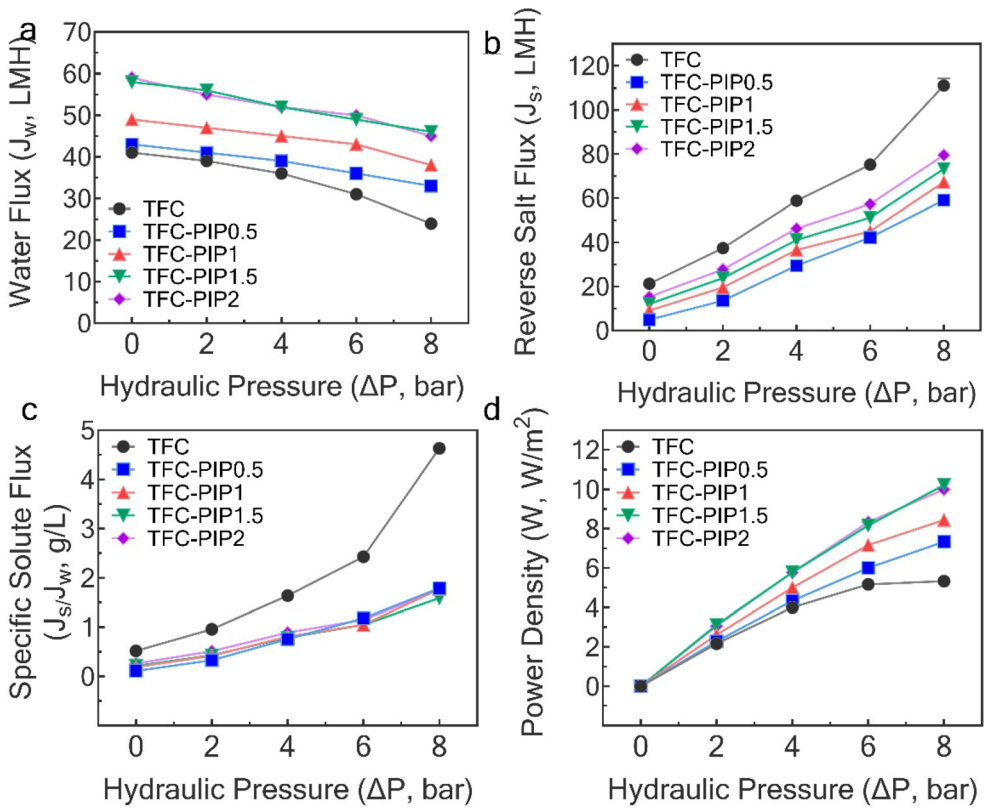

Fig. 7 (a) Water flux (J_w), (b) reverse salt flux (J_s), (c) specific solute flux (J_s/J_w), and (d) power density (W) for the TFC and TFC-PIP membranes, tested in the PRO process. PRO performance was obtained using DI water as feed solution and 1.0 M NaCl as draw solution. A dashed horizontal line in panel (d) indicates the industrial target for commercial feasibility in PRO operations.

TFC and TFC-PIP membranes. The power density generated by all membranes increased by increasing the applied pressure. The overall power density of the TFC-PIP1.5 and TFC-PIP2 membranes was higher than that of the pristine TFC membrane. The TFC-PIP1.5 and TFC-PIP2 membranes achieved maximum power densities of 10.2 and 10 W m^{-2}, respectively, while the TFC membrane showed a maximum power density of 5.3 W m^{-2} at the same hydraulic pressure (8 bar). These results notably surpass the power densities previously reported for PRO membranes using a 1 M NaCl draw solution, exceeding the critical benchmark of 5 W m^{-2} necessary for the economic feasibility of the PRO process.[111,112]

Moreover, the long-term operational stability of the membranes was assessed through continuous monitoring of water flux, specific solute flux, and power density under a sustained pressure of 8 bar for 8 hours, and the results are depicted in Fig. 8. The membranes demonstrated stable flux rates: 24 ± 0.4 LMH for TFC, 33 ± 0.5 LMH for TFC-PIP0.5, 38 ± 0.8 for TFC-PIP1, and 46 ± 0.9 LMH for TFC-PIP1.5, and 45 ± 0.9 for TFC-PIP2. Furthermore, the power densities remained consistent throughout the operation, recorded as 5.3 ± 0.1 W m^{-2} for the TFC membrane, 7.3 ± 0.2 W m^{-2} for the TFC-PIP0.5 membrane, 8.4 ± 0.2 for TFCPIP-1, 10.2 ± 0.2 for TFC-PIP1.5, and 10.0 ± 0.2 W m^{-2} for the TFC-PIP2 membrane. The specific solute fluxes also remained stable during the testing period, indicating that the membrane effectively retains its selectivity while allowing high water flux. This stability is crucial for reducing operational costs and maintaining membrane efficiency over time. The favorable trade-off between high water flux and low reverse salt flux ensures that energy extraction remains efficient, making the 1.5 wt% PIP concentration an optimal choice for long-term operations. However, when the pressure was increased beyond 8 bar, a significant rise in specific salt flux was noted, which is likely due to membrane deformation as it approached the burst pressure of 9 bar.[17,113] These results are instrumental in understanding the membranes' performance and resilience under prolonged high-pressure conditions. When operating at pressures below the burst threshold, minor compaction effects may occur, but these effects are fully reversible.[114] Under these conditions, time-dependent deformations are unlikely to manifest, as the substrate does not experience permanent deformation at lower pressures. However, when pressures exceed the mechanical limits of the substrate (*i.e.*, the burst pressure), gradual deformation and potential performance loss may occur over time. To mitigate potential degradation, several strategies are recommended, including the reinforcement of the membrane's support structure with nanomaterials,[115,116] optimization of the support layer's morphology,[10] and careful operation below critical pressure thresholds.[114] By incorporating these strategies, long-term membrane performance can be effectively maintained, even under extended high-pressure conditions.

3.4. Comparison of the power generation efficiency among different PRO flat sheet membranes

In this study, the TFC-PIP1.5 membrane demonstrated a power density of 10.2 W m^{-2} at an 8 bar hydraulic pressure using 1 M NaCl as draw solution and DI water as feed solution, respectively. The membrane's remarkable performance at such a low pressure suggests an energy-efficient approach, a crucial aspect for the practical implementation and economic feasibility of PRO technology.

Fig. 9 introduces an index ratio of power density to applied hydraulic pressure. Comparison of this index for the

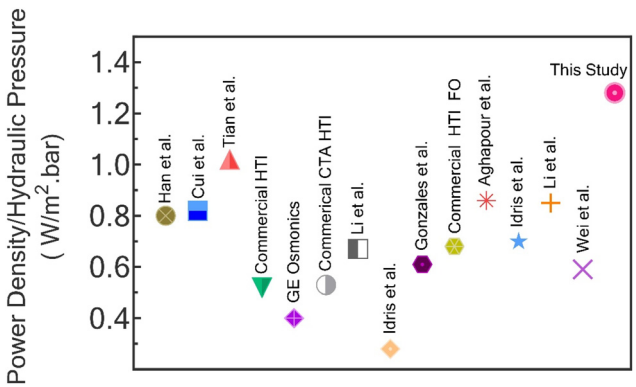

Fig. 9 Comparison of power generation performance of the TFC-PIP1.5 and various reported flat sheet membranes.[14,113,117–126] PRO performance was measured using DI water as feed and 1.0 M NaCl solution as draw solution.

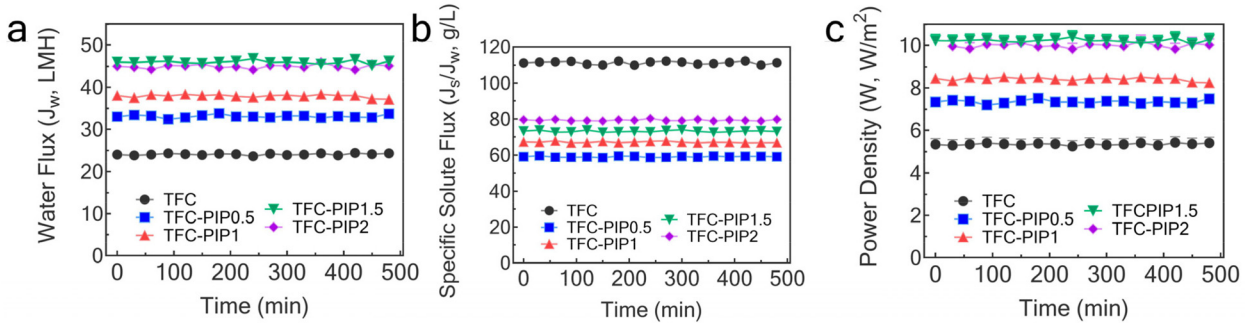

Fig. 8 Long-term PRO performance of the TFC and TFN membranes. (a) Water flux (J_w), (b) specific solute flux (J_s/J_w), and (c) power density (W); (testing condition: DI water as feed, 1.0 M NaCl as draw solution, 25 ± 0.5 °C, 8 bar, and dosing every 15–60 min to regulate the conductivity).

This journal is © The Royal Society of Chemistry 2024

TFC-PIP1.5 membrane against other reported PRO membranes[14,113,117–126] under identical operating conditions reveals the superior performance of our membrane. The results of this study is encouraging, yet they underscore the necessity for further research in developing specialty PRO membranes. Specifically, there is a need to enhance the mechanical strength of the support layer, a critical factor in ensuring the durability of PRO operations under elevated pressures.[63] High pressures are preferable, as they result in more power generation. For instance, a pressure of approximately 22 bar is deemed optimal when using a 1 M solution (such as brine from RO) as the draw solution and river water with a 0.01 M concentration as the feed solution.

3.5. Life cycle assessment of the membranes synthesis

3.5.1. Cumulative energy demand (CED). The data presented in Fig. 10a indicates a comparative CED analysis of different membranes synthesized for the PRO system. The TFC membrane is set as the 100% reference point for normalized impact. The introduction of PIP in synthesizing co-polyamide membranes results in varied energy demands for the membrane fabrication process. As PIP concentration increases from 0.5 to 2.0, there is an overall trend of decreasing CED, suggesting enhanced sustainability of membrane production. The lowest CED is observed for TFC-PIP1.5, indicating an optimal trade-off between performance and energy requirements. Fig. 10b indicates the energy mix used to synthesize each membrane. The TFC membrane primarily relies on fossil fuels, with a significant 97% impact. The introduction of PIP alters this energy mix. TFC-PIP0.5 shows a slight reduction in fossil fuel reliance. As the PIP content increases, the proportion of nuclear and renewable energy sources, including renewable biomass, water, wind, solar, and geothermal, gradually increases, suggesting a shift towards a more sustainable energy profile in membrane synthesis. The TFC-PIP2 membrane exhibits the highest diversity in energy sources, indicating the least reliance on fosil fuels and the most sustainable energy usage among the membranes studied.

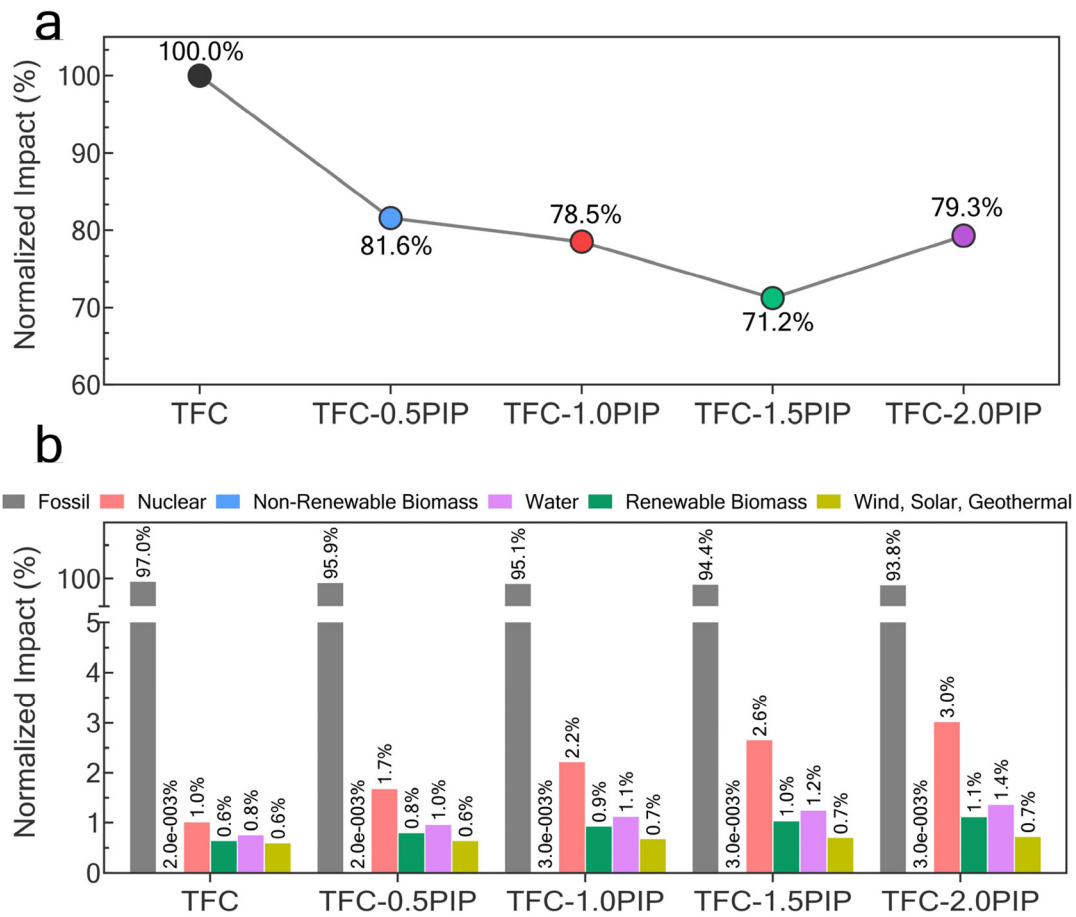

Fig. 10 Comparative cumulative energy demand (CED) analysis of TFC and TFC-PIP membranes for PRO Systems. (a) Normalized CED of membranes, which indicates a decrease in normalized CED with an increase in PIP concentration, implying enhanced sustainability in membrane production—TFC-PIP1.5 being the most efficient. (b) The energy mix of the membranes' production. This section details the shift in energy mix from heavy reliance on fossil fuels in the TFC membrane to a more diversified and sustainable profile in TFC-PIP2, emphasizing the improved use of renewable sources like wind, solar, and geothermal energy.

Building on this analysis, shifting from fossil fuel reliance in TFC membranes to a more sustainable energy mix in Co-PA membranes provides significant environmental advantages. To further optimize this transition, bio-based materials could be incorporated to reduce petrochemical dependency,[127] energy efficiency could be improved in both production and operational phases,[110] and membrane lifespan could be extended through enhanced durability.[128,129] Additionally, renewable energy sources, such as solar and wind, could be integrated into industrial applications.[130] These proposed optimizations would greatly reduce the environmental footprint of Co-PA membranes, while supporting global efforts toward cleaner, renewable energy solutions.

3.5.2. Environmental impacts. Fig. 11 analyzes the environmental impacts of membrane synthesis. The numerical data indicates that the base TFC membrane establishes a benchmark with a score of 100 across most categories. In the Acidification category, the TFC-PIP1.5 membrane shows the most significant reduction compared to the baseline TFC membrane, decreasing to 82.2%. In contrast, TFC-PIP2 shows an increase to 94.3%. For Carcinogenics, the TFC-PIP1.5 membrane also has the lowest impact at 76.2%, while TFC-PIP0.5 and TFC-PIP1 show similar values. Ecotoxicity steadily decreases with increasing PIP content, with TFC-PIP1.5 reaching the lowest at 62.9%. Eutrophication follows a similar trend, with TFC-PIP1.5 at 61.9%. Fossil Fuel Depletion is least impacted by TFC-PIP1.5 at 66.8% but increases again for TFC-PIP2. Global Warming impact increases with higher PIP, peaking at TFC-PIP2. Non-Carcinogenics and Ozone Depletion impacts are lowest for TFC-PIP1.5, while Respiratory Effects and Smog see an increase in impact with higher PIP concentrations, both peaking at TFC-PIP2.

Comparing TFC and TFC-PIP1.5 membranes, TFC serves as the baseline with the highest environmental impact scores across all categories. TFC-PIP1.5 significantly reduces this impact, most notably in ecotoxicity (62.9%), eutrophication (61.9%), and fossil fuel depletion (66.8%), indicating a substantial environmental benefit. Additionally, TFC-PIP1.5 performs better in the categories of Acidification and Carcinogenics, showing a more environmentally benign profile overall. These reductions in environmental impact highlight the effectiveness of incorporating PIP into membrane synthesis for a more sustainable approach.

The superior osmotic performance of Co-PA membranes contributes to sustainability by offsetting the higher initial energy input. This is achieved by reducing the overall number of membranes required and increasing operational efficiency. As detailed above, TFC-PIP1.5 membrane require 48% less surface area to generate an equivalent energy output (500 000 kW h over 10 days) compared to TFC membrane. This substantial reduction in material usage not only boosts efficiency but also significantly lowers the long-term environmental footprint. These improvements underscore the environmental advantages of Co-PA membranes across both production and operational phases, positioning them as a sustainable alternative to existing membranes.

3.5.3. Effect of production scale-up on the LCA. Fig. 12a shows the comparative analysis of CED results for large-scale TFC-PIP1.5 (L-TFC-PIP1.5) *versus* lab-scale TFC-PIP1.5. Results

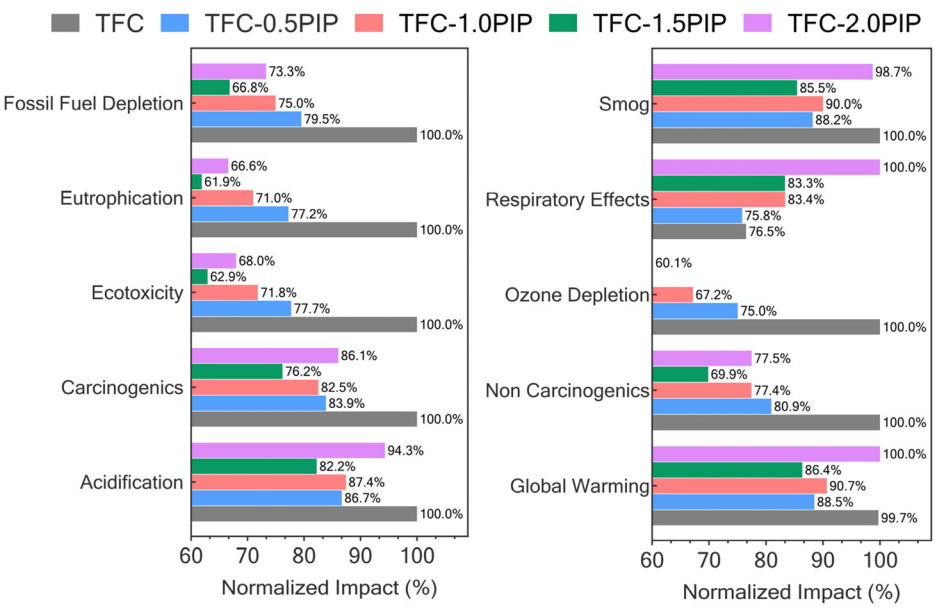

Fig. 11 Environmental impact assessment of TFC and PIP-Enhanced TFC Membranes in Membrane Synthesis. The graph benchmarks the TFC membrane at 100% across various environmental categories. TFC-PIP1.5 shows marked reductions in Acidification (82.2%), Carcinogenics (76.2%), Ecotoxicity (62.9%), Eutrophication (61.9%), and Fossil Fuel Depletion (66.8%). However, the TFC-PIP2 sees an increased impact in Acidification, Global Warming, Respiratory Effects, and Smog, with scores peaking at 94.3% and 100%, respectively. This comparison underscores TFC-PIP1.5's reduced environmental burden, advocating for its sustainable synthesis approach.

This journal is © The Royal Society of Chemistry 2024

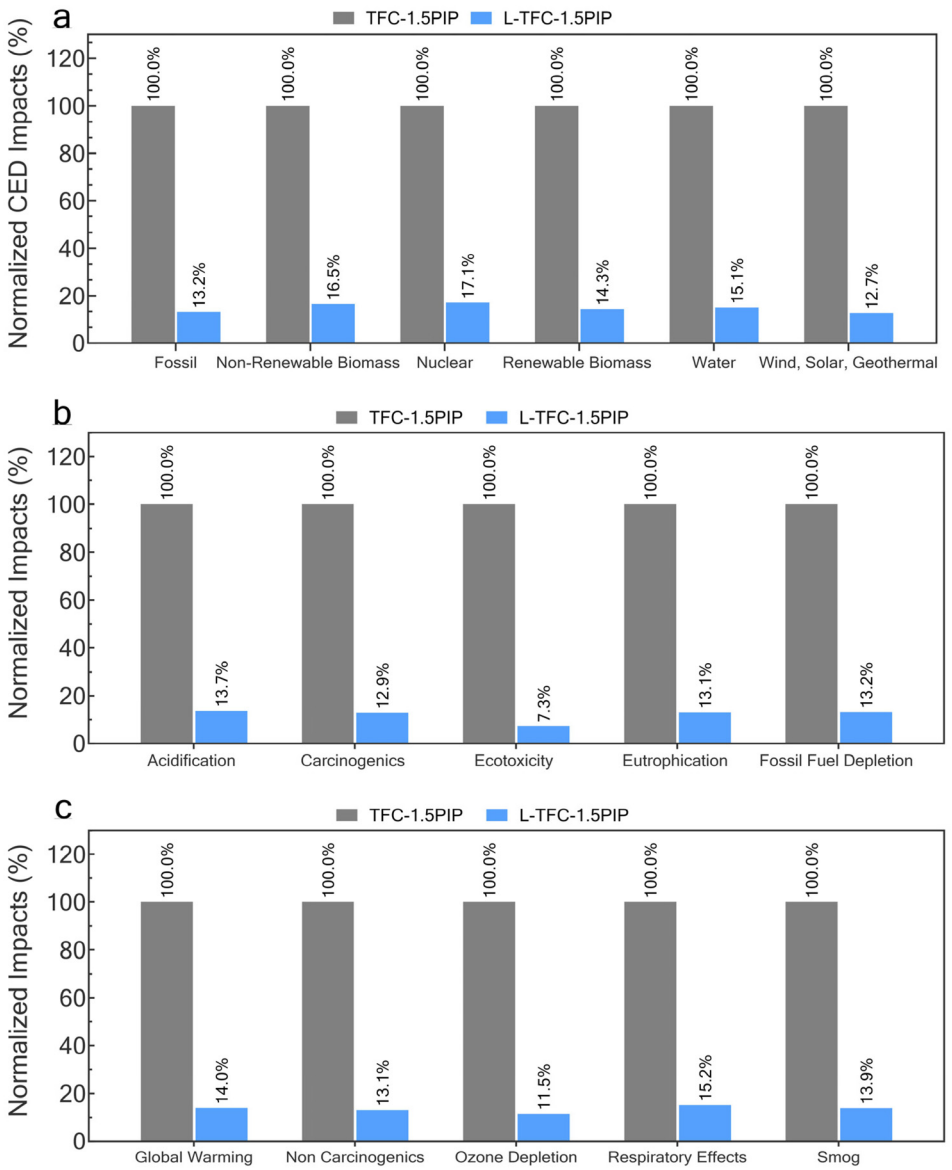

Fig. 12 Normalized environmental impacts of lab-scale *versus* large-scale TFC-PIP1.5 membrane synthesis. (a) CED results, (b), and (c) environmental impacts result. Results illustrate a drastic reduction in environmental impacts when transitioning from lab-scale to large-scale production. In all categories, the large-scale impacts are significantly lower, with the greatest improvement shown in Ecotoxicity at 7.3%. This data underscores the sustainability advantages of large-scale membrane manufacturing, reinforcing the environmental efficacy of upscaling production processes.

show a significant reduction in environmental impact for large-scale production. With all values normalized to the lab-scale membrane, the large-scale version dramatically lowers the impact on every front: only 13.19% for fossil fuels, 16.529% for non-renewable biomass, 17.119% for nuclear, 14.339% for renewable biomass, 15.068% for water, and 12.695% for wind, solar, and geothermal. This substantial decrease suggests that upscaling the membrane production process is not only more energy-efficient but also potentially reduces the overall environmental footprint. The transition from lab-scale to large-scale synthesis of TFC-PIP1.5 membranes exhibits notable environmental benefits (Fig. 12b and c). The large-scale production significantly reduces environmental impacts across all categories when normalized against lab-scale values set at 100%. The impacts on Acidification, Carcinogenics, and Eutrophication are reduced to approximately 13% of the lab-scale values. Even more pronounced is the reduction in Ecotoxicity, dropping to 7.3%. This indicates that upscaling the membrane fabrication process significantly enhances environmental performance, aligning with sustainable industrial practice principles.

Further supporting this, life cycle assessment results demonstrate that Co-PA membranes provide significant environmental benefits at industrial scales. These advantages

include reduced material usage, lower operational energy consumption, and a decrease in global warming potential. Waste generation from Co-PA membrane fabrication has been optimized through solvent recovery, the use of less hazardous chemicals, and water reuse. For example, the phase separation technique employed in substrate membrane preparation effectively minimizes both water and solvent waste through an optimized recovery system. These advancements, as demonstrated by the scale-up production data, highlight the superior sustainability and efficiency of large-scale TFC-PIP1.5 membrane fabrication compared to the lab-scale version.

4. Conclusion

This study presents a significant advancement in PRO technology by developing novel Co-PA membranes created from MPD and PIP. These membranes, particularly with the incorporation of 1.5 wt% PIP (TFC-PIP1.5) exhibited remarkable improvements in water permeability and salt rejection, critical for an efficient PRO process. The integration of PIP enhanced the hydrophilicity of the membranes, resulting in an impressive power density of 10.2 W m^{-2}, which is about a 92% increase compared to the 5.3 W m^{-2} of pristine TFC membranes. As revealed by SEM and AFM imaging, the structural modifications due to PIP integration led to increased surface roughness, thereby creating additional surface area and elevating water flux to 58 LMH in PRO mode, representing a 41.5% increase over pristine TFC membranes. XPS analysis further demonstrated that introducing PIP leads to increased cross-linking in TFC-PIP membranes, which results in a 36.7% reduction in reverse salt flux for TFC-PIP1.5 compared to the pristine TFC membrane. The addition of PIP not only improved the physicochemical properties of the membranes but also bolstered the sustainability aspect of the technology. A life cycle assessment confirmed the environmental advantages of these innovative membranes. The results of this study highlight the potential of Co-PA membranes to revolutionize PRO technology, offering promising avenues for sustainable energy generation and effective water treatment. These membranes hold significant potential for large-scale, real-world applications in energy production and water treatment, showing improved performance compared to conventional membranes. However, several challenges must be addressed for commercial viability, including scaling up production, optimizing long-term operational stability, and conducting comprehensive economic assessments. Future research should focus on overcoming these barriers through various approaches such as exploring broader monomer selections and refining fabrication techniques. By addressing these challenges, Co-PA membranes could contribute to more efficient and sustainable solutions for energy generation and water treatment in critical global sectors. This research lays the foundation for further investigations and optimizations in membrane materials and configurations to maximize the efficiency and sustainability of PRO systems.

Author contributions

Sadegh Aghapour Aktij: conceptualization, data curation, formal analysis, investigation, methodology, validation, writing – original draft. Mostafa Dadashi Firouzjaei: conceptualization, data curation, formal analysis, investigation, methodology, project administration, resources, supervision, validation, writing – original draft. Mohsen Pilevar: data curation, formal analysis, investigation. Asad Asad Asad: data curation, formal analysis, investigation. Ahmad Rahimpour: conceptualization, data curation, formal analysis, investigation, methodology, validation, writing – review and editing. Mark Elliott: resources, writing – review & editing. João B.P. Soares: conceptualization, methodology, project administration, resources, supervision, validation, writing – review & editing. Mohtada Sadrzadeh: conceptualization, data curation, formal analysis, investigation, methodology, project administration, resources, supervision, validation, writing – review & editing.

Data availability

The data supporting the findings of this study are available upon reasonable request from the corresponding author. Any restrictions on data access, such as ethical considerations or confidentiality agreements, have been clearly stated. The article and its ESI† files include all other relevant data.

Conflicts of interest

■■■■ Q4

Acknowledgements

This research was financially supported by the Natural Science and Engineering Research Council of Canada (NSERC) and Canada's Oil Sands Innovation Alliance (COSIA), whose contributions are gratefully acknowledged. Sadegh Aghapour Aktij appreciates the financial support received from the Killam Centre for Advanced Studies *via* the Izaak Walton Killam Memorial Scholarship, and the Alberta Innovates Graduate Student Scholarship (AIGSS), sponsored by Alberta Innovates of the Alberta government, Canada. Q5

References

1 A. Carlino, M. Wildemeersch, C. J. Chawanda, M. Giuliani, S. Sterl, W. Thiery, *et al.*, Declining cost of renewables and climate change curb the need for African hydropower expansion, *Science*, 2023, **381**(6658), eadf5848. Q6

2 B. J. Van Ruijven, E. De Cian and I. Sue Wing, Amplification of future energy demand growth due to climate change, *Nat. Commun.*, 2019, **10**(1), 2762. Q7

 This journal is © The Royal Society of Chemistry 2024

3 P. Wang, Y. Yang, D. Xue, L. Ren, J. Tang, L. R. Leung, *et al.*, Aerosols overtake greenhouse gases causing a warmer climate and more weather extremes toward carbon neutrality, *Nat. Commun.*, 2023, **14**(1), 7257.

4 H. Sahin, A. Solomon, A. Aghahosseini and C. Breyer, Systemwide energy return on investment in a sustainable transition towards net zero power systems, *Nat. Commun.*, 2024, **15**(1), 208.

5 S. Sengupta, P. J. Adams, T. A. Deetjen, P. Kamboj, S. D'Souza, R. Tongia, *et al.*, Subnational implications from climate and air pollution policies in India's electricity sector, *Science*, 2022, **378**(6620), eabh1484.

6 X. Huang, V. Srikrishnan, J. Lamontagne, K. Keller and W. Peng, Effects of global climate mitigation on regional air quality and health, *Nat. Sustainability*, 2023, 1–13.

7 M. Rastgar, K. Moradi, C. Burroughs, A. Hemmati, E. Hoek and M. Sadrzadeh, Harvesting blue energy based on salinity and temperature gradient: challenges, solutions, and opportunities, *Chem. Rev.*, 2023, **123**(16), 10156–10205.

8 B. Yang, J. Yu and T. Ma, A charge-free and membrane-free hybrid capacitive mixing system for salinity gradient energy harvesting, *J. Mater. Chem. A*, 2023, **11**(7), 3388–3398.

9 A. Parra, M. Noriega, L. Yokoyama and M. Bagajewicz, Does Pressure-Retarded Osmosis Help Reverse Osmosis in Desalination?, *Ind. Eng. Chem. Res.*, 2021, **60**(11), 4366–4374.

10 N.-N. Bui and J. R. McCutcheon, Nanofiber supported thin-film composite membrane for pressure-retarded osmosis, *Environ. Sci. Technol.*, 2014, **48**(7), 4129–4136.

11 S. A. Aktij, M. D. Firouzjaei, S. A. Haddadi, P. Karami, A. Taghipour, M. Yassari, *et al.*, Metal-organic frameworks' latent potential as High-Efficiency osmotic power generators in Thin-Film nanocomposite membranes, *Chem. Eng. J.*, 2023, 148384.

12 Q. She, J. Wei, N. Ma, V. Sim, A. G. Fane, R. Wang, *et al.*, Fabrication and characterization of fabric-reinforced pressure retarded osmosis membranes for osmotic power harvesting, *J. Membr. Sci.*, 2016, **504**, 75–88.

13 G. Han, S. Zhang, X. Li and T.-S. Chung, Progress in pressure retarded osmosis (PRO) membranes for osmotic power generation, *Prog. Polym. Sci.*, 2015, **51**, 1–27.

14 Y. Li, R. Wang, S. Qi and C. Tang, Structural stability and mass transfer properties of pressure retarded osmosis (PRO) membrane under high operating pressures, *J. Membr. Sci.*, 2015, **488**, 143–153.

15 S. N. Rahman, H. Saleem and S. J. Zaidi, Progress in membranes for pressure retarded osmosis application, *Desalination*, 2023, **549**, 116347.

16 Y. Shi, M. Zhang, H. Zhang, F. Yang, C. Y. Tang and Y. Dong, Recent development of pressure retarded osmosis membranes for water and energy sustainability: A critical review, *Water Res.*, 2021, **189**, 116666.

17 J. H. Kim, S. J. Moon, S. H. Park, M. Cook, A. G. Livingston and Y. M. Lee, A robust thin film composite membrane incorporating thermally rearranged polymer support for organic solvent nanofiltration and pressure retarded osmosis, *J. Membr. Sci.*, 2018, **550**, 322–331.

18 B. Yuan, S. Zhao, P. Hu, J. Cui and Q. J. Niu, Asymmetric polyamide nanofilms with highly ordered nanovoids for water purification, *Nat. Commun.*, 2020, **11**(1), 6102.

19 K. Huang, K. P. Reber, M. D. Toomey, J. A. Howarter and A. D. Shah, Reactivity of the polyamide membrane monomer with free chlorine: role of bromide, *Environ. Sci. Technol.*, 2021, **55**(4), 2575–2584.

20 M. Dadashi Firouzjaei, J. Clayton, H. Jafarian, A. Arabi Shamsabadi, A. Thakur, R. Todd, *et al.*, A perspective on MXene-enhanced biofiltration-membrane water reuse treatment systems: A review and experimental validation, *Desalination*, 2025, **593**, 118198.

21 U. Baig and A. Waheed, Exploiting interfacial polymerization to fabricate hyper-cross-linked nanofiltration membrane with a constituent linear aliphatic amine for freshwater production, *npj Clean Water*, 2022, **5**(1), 46.

22 A. Waheed, U. Baig, A. Matin, S. M. S. Jillani, N. A. Qasem and I. H. Aljundi, Synthesis of co-polyamide reverse osmosis membrane constituting a linear aliphatic triamine and *m*-phenylenediamine for enhanced desalination performance, *Desalination*, 2023, **549**, 116311.

23 Y. Chen, Q. J. Niu, Y. Hou and H. Sun, Effect of interfacial polymerization monomer design on the performance and structure of thin film composite nanofiltration and reverse osmosis membranes: A review, *Sep. Purif. Technol.*, 2023, 125282.

24 D. Lu, Z. Yao, L. Jiao, M. Waheed, Z. Sun and L. Zhang, Separation mechanism, selectivity enhancement strategies and advanced materials for mono-/multivalent ion-selective nanofiltration membrane, *Adv. Membr.*, 2022, **2**, 100032.

25 C. Ji, Z. Zhai, C. Jiang, P. Hu, S. Zhao, S. Xue, *et al.*, Recent advances in high-performance TFC membranes: A review of the functional interlayers, *Desalination*, 2021, **500**, 114869.

26 P. Karami, B. Khorshidi, J. B. Soares and M. Sadrzadeh, Fabrication of highly permeable and thermally stable reverse osmosis thin film composite polyamide membranes, *ACS Appl. Mater. Interfaces*, 2019, **12**(2), 2916–2925.

27 A. K. Ghosh, B.-H. Jeong, X. Huang and E. M. V. Hoek, Impacts of reaction and curing conditions on polyamide composite reverse osmosis membrane properties, *J. Membr. Sci.*, 2008, **311**(1), 34–45.

28 M. R. Esfahani, S. A. Aktij, Z. Dabaghian, M. D. Firouzjaei, A. Rahimpour, J. Eke, *et al.*, Nanocomposite membranes for water separation and purification: Fabrication, modification, and applications, *Sep. Purif. Technol.*, 2019, **213**, 465–499.

29 P. Goh and A. Ismail, Chemically functionalized polyamide thin film composite membranes: The art of chemistry, *Desalination*, 2020, **495**, 114655.

30 P. Karami, S. A. Aktij, B. Khorshidi, M. D. Firouzjaei, A. Asad, M. Elliott, *et al.*, Nanodiamond-decorated thin film composite membranes with antifouling and antibacterial properties, *Desalination*, 2022, **522**, 115436.

31 S. Siahtiri, A. A. Sahraei, A. H. Mokarizadeh, M. Baghani, M. Bodaghi and M. Baniassadi, Influence of Curing Agents Molecular Structures on Interfacial Characteristics of Graphene/Epoxy Nanocomposites: A Molecular Dynamics Framework, *Macromol. Mater. Eng.*, 2023, **308**(8), 2300030.

32 A. Rahimpour, S. F. Seyedpour, S. Aghapour Aktij, M. Dadashi Firouzjaei, A. Zirehpour, A. Arabi Shamsabadi, *et al.*, Simultaneous Improvement of Antimicrobial, Antifouling, and Transport Properties of Forward Osmosis Membranes with Immobilized Highly-Compatible Polyrhodanine Nanoparticles, *Environ. Sci. Technol.*, 2018, **52**(9), 5246–5258.

33 H. Shen, S. Wang, H. Xu, Y. Zhou and C. Gao, Preparation of polyamide thin film nanocomposite membranes containing silica nanoparticles via an *in situ* polymerization of SiCl4 in organic solution, *J. Membr. Sci.*, 2018, **565**, 145–156.

34 S. A. Aktij, M. Hosseininejad, M. Dadashi Firouzjaei, S. Farhadi, M. Elliott, A. Rahimpour, *et al.*, High permselectivity and performance of tuned nanofiltration membranes by merging carbon nitride derivatives as interphase layer for efficient water treatment, *J. Water Process Eng.*, 2023, **56**, 104432.

35 G. Gong, P. Wang, Z. Zhou and Y. Hu, New Insights into the Role of an Interlayer for the Fabrication of Highly Selective and Permeable Thin-Film Composite Nanofiltration Membrane, *ACS Appl. Mater. Interfaces*, 2019, **11**(7), 7349–7356.

36 P. Karami, M. M. Haque Mizan, B. Khorshidi, S. Aghapour Aktij, A. Rahimpour, J. B. P. Soares, *et al.*, Novel Forward Osmosis Membranes Engineered with Polydopamine/Graphene Oxide Interlayers: Synergistic Impact of Monomer Reactivity and Hydrophilic Interlayers, *Ind. Eng. Chem. Res.*, 2023, **62**(30), 11965–11976.

37 H.-g. Choi, A. A. Shah, S.-E. Nam, Y.-I. Park and H. Park, Thin-film composite membranes comprising ultrathin hydrophilic polydopamine interlayer with graphene oxide for forward osmosis, *Desalination*, 2019, **449**, 41–49.

38 H. Jafarian, M. Dadashi Firouzjaei, S. Aghapour Aktij, A. Aghaei, M. Pilevar Khomami, M. Elliott, *et al.*, Synthesis of heterogeneous metal organic Framework-Graphene oxide nanocomposite membranes for water treatment, *Chem. Eng. J.*, 2023, **455**, 140851.

39 H. Huang, S. Lin, L. Zhang and H. La, Chlorine-resistant polyamide reverse osmosis membrane with monitorable and regenerative sacrificial layers, *ACS Appl. Mater. Interfaces*, 2017, **9**(11), 10214–10223.

40 S.-M. Xue, C.-H. Ji, Z.-L. Xu, Y.-J. Tang and R.-H. Li, Chlorine resistant TFN nanofiltration membrane incorporated with octadecylamine-grafted GO and fluorine-containing monomer, *J. Membr. Sci.*, 2018, **545**, 185–195.

41 M. Pejman, M. D. Firouzjaei, S. A. Aktij, P. Das, E. Zolghadr, H. Jafarian, *et al.*, Improved antifouling and antibacterial properties of forward osmosis membranes through surface modification with zwitterions and silver-based metal organic frameworks, *J. Membr. Sci.*, 2020, **611**, 118352.

42 M. Dadashi Firouzjaei, M. Pejman, M. S. Gh, S. A. Aktij, E. Zolghadr, A. Rahimpour, *et al.*, Functionalized polyamide membranes yield suppression of biofilm and planktonic bacteria while retaining flux and selectivity, *Sep. Purif. Technol.*, 2022, **282**, 119981.

43 S. Abdikheibari, W. Lei, L. F. Dumée, N. Milne and K. Baskaran, Thin film nanocomposite nanofiltration membranes from amine functionalized-boron nitride/polypiperazine amide with enhanced flux and fouling resistance, *J. Mater. Chem. A*, 2018, **6**(25), 12066–12081.

44 H. Wang, L. Li, X. Zhang and S. Zhang, Polyamide thin-film composite membranes prepared from a novel triamine 3, 5-diamino-N-(4-aminophenyl)-benzamide monomer and *m*-phenylenediamine, *J. Membr. Sci.*, 2010, **353**(1–2), 78–84.

45 Y.-J. Tang, Z.-L. Xu, S.-M. Xue, Y.-M. Wei and H. Yang, A chlorine-tolerant nanofiltration membrane prepared by the mixed diamine monomers of PIP and BHTTM, *J. Membr. Sci.*, 2016, **498**, 374–384.

46 P. Jin, M. Robeyn, J. Zheng, S. Yuan and B. Van der Bruggen, Tailoring charged nanofiltration membrane based on non-aromatic Tris (3-aminopropyl) amine for effective water softening, *Membranes*, 2020, **10**(10), 251.

47 P. Sarkar, S. Ray, B. Sutariya, J. C. Chaudhari and S. Karan, Precise separation of small neutral solutes with mixed-diamine-based nanofiltration membranes and the impact of solvent activation, *Sep. Purif. Technol.*, 2021, **279**, 119692.

48 X. Wang, H. Ma, B. Chu and B. S. Hsiao, Thin-film nanofibrous composite reverse osmosis membranes for desalination, *Desalination*, 2017, **420**, 91–98.

49 C. Yang, W. Xu, Y. Nan and Y. Wang, Novel solvent-resistant nanofiltration membranes using MPD co-crosslinked polyimide for efficient desalination, *J. Membr. Sci.*, 2020, **616**, 118603.

50 X. Cheng, Q. Pan, H. Tan, W. Liu, Y. Shi, S. Du, *et al.*, The construction of an efficient magnesium–lithium separation thin film composite membrane with dual aqueous-phase monomers (PIP and MPD), *RSC Adv.*, 2023, **13**(32), 22113–22121.

51 B. Vyas and P. Ray, Preparation of nanofiltration membranes and relating surface chemistry with potential and topography: Application in separation and desalting of amino acids, *Desalination*, 2015, **362**, 104–116.

52 I. C. Kim, J. Jegal and K. H. Lee, Effect of aqueous and organic solutions on the performance of polyamide thin–film–composite nanofiltration membranes, *J. Polym. Sci., Part B: Polym. Phys.*, 2002, **40**(19), 2151–2163.

53 S. Hellweg, E. Benetto, M. A. Huijbregts, F. Verones and R. Wood, Life-cycle assessment to guide solutions for the

This journal is © The Royal Society of Chemistry 2024

triple planetary crisis, *Nat. Rev. Earth Environ.*, 2023, **4**(7), 471–486.
54 S. Sala, A. M. Amadei, A. Beylot and F. Ardente, The evolution of life cycle assessment in European policies over three decades, *Int. J. Life Cycle Assess.*, 2021, **26**, 2295–2314.
55 M. Dadashi Firouzjaei, S. K. Nemani, M. Sadrzadeh, E. K. Wujcik, M. Elliott and B. Anasori, Life–Cycle Assessment of Ti3C2Tx MXene Synthesis, *Adv. Mater.*, 2023, **35**(31), 2300422.
56 K. Moradi, M. D. Firouzjaei, M. Elliott and M. Sadrzadeh, Lifecycle assessment of membrane synthesis for the application of thermo-osmotic energy conversion process, *Case Stud. Chem. Environ. Eng.*, 2024, **10**, 100847.
57 P. Karami, S. A. Aktij, B. Khorshidi, M. D. Firouzjaei, A. Asad, M. Elliott, *et al.*, Nanodiamond-decorated thin film composite membranes with antifouling and antibacterial properties, *Desalination*, 2022, **522**, 115436.
58 M. Mardani, S. Siahtiri, M. Besati, M. Baghani, M. Baniassadi and A. M. Nejad, Microencapsulation of natural products using spray drying; an overview, *J. Microencapsulation*, 2024, 1–30.
59 M. D. Firouzjaei, M. Pejman, M. S. Gh, S. A. Aktij, E. Zolghadr, A. Rahimpour, *et al.*, Functionalized polyamide membranes yield suppression of biofilm and planktonic bacteria while retaining flux and selectivity, *Sep. Purif. Technol.*, 2022, **282**, 119981.
60 M. Pejman, M. D. Firouzjaei, S. A. Aktij, P. Das, E. Zolghadr, H. Jafarian, *et al.*, Improved antifouling and antibacterial properties of forward osmosis membranes through surface modification with zwitterions and silver-based metal organic frameworks, *J. Membr. Sci.*, 2020, **611**, 118352.
61 G. Han, P. Wang and T.-S. Chung, Highly robust thin-film composite pressure retarded osmosis (PRO) hollow fiber membranes with high power densities for renewable salinity-gradient energy generation, *Environ. Sci. Technol.*, 2013, **47**(14), 8070–8077.
62 K. Touati and F. Tadeo, Pressure retarded osmosis as renewable energy source, *Pressure Retarded Osmosis*, Elsevier, 2017, 1–54.
63 S. J. Kwon, K. Park, D. Y. Kim, M. Zhan, S. Hong and J.-H. Lee, High-performance and durable pressure retarded osmosis membranes fabricated using hydrophilized polyethylene separators, *J. Membr. Sci.*, 2021, **619**, 118796.
64 S. F. Seyedpour, M. Dadashi Firouzjaei, A. Rahimpour, E. Zolghadr, A. Arabi Shamsabadi, P. Das, *et al.*, Toward sustainable tackling of biofouling implications and improved performance of TFC FO membranes modified by Ag-MOF nanorods, *ACS Appl. Mater. Interfaces*, 2020, **12**(34), 38285–38298.
65 S. A. Aktij, A. Rahimpour and A. Figoli, Low content nano-polyrhodanine modified polysulfone membranes with superior properties and their performance for wastewater treatment, *Environ. Sci.: Nano*, 2017, **4**(10), 2043–2054.
66 Y.-N. Kwon and J. O. Leckie, Hypochlorite degradation of crosslinked polyamide membranes: II. Changes in hydrogen bonding behavior and performance, *J. Membr. Sci.*, 2006, **282**(1–2), 456–464.
67 G. Socrates, *Infrared characteristic group frequencies: tables and charts*, No Title, 1995.
68 J. Shen, G. Wang, X. You, B. Shi, J. Xue, J. Yuan, *et al.*, Thermal-facilitated interfacial polymerization toward high-performance polyester desalination membrane, *J. Mater. Chem. A*, 2021, **9**(13), 8470–8479.
69 B. Suart, Infrared spectroscopy: Fundamental and applications, Google Scholar, 2004.
70 D. Wu, J. Martin, J. R. Du, Y. Zhang, D. Lawless and X. Feng, Effects of chlorine exposure on nanofiltration performance of polyamide membranes, *J. Membr. Sci.*, 2015, **487**, 256–270.
71 A. K. Shukla, J. Alam, M. S. Alhoshan, F. A. A. Ali, U. Mishra and A. A. Hamid, Thin-film nanocomposite membrane incorporated with porous Zn-based metal–organic frameworks: toward enhancement of desalination performance and chlorine resistance, *ACS Appl. Mater. Interfaces*, 2021, **13**(24), 28818–28831.
72 Y.-l. Liu, Y.-y. Zhao, X.-m. Wang, X.-h. Wen, X. Huang and Y. F. Xie, Effect of varying piperazine concentration and post-modification on prepared nanofiltration membranes in selectively rejecting organic micropollutants and salts, *J. Membr. Sci.*, 2019, **582**, 274–283.
73 S. Karan, Z. Jiang and A. G. Livingston, Sub–10 nm polyamide nanofilms with ultrafast solvent transport for molecular separation, *Science*, 2015, **348**(6241), 1347–1351.
74 S. Ibrahim, M. Mohammadi Ghaleni, A. M. Isloor, M. Bavarian and S. Nejati, Poly (Homopiperazine–Amide) thin-film composite membrane for nanofiltration of heavy metal ions, *ACS Omega*, 2020, **5**(44), 28749–28759. Q14
75 J. Sun, Q. Zhang, W. Xue, W. Ding, K. Zhang and S. Wang, An economical and simple method for preparing highly permeable and chlorine-resistant reverse osmosis membranes with potential commercial applications, *RSC Adv.*, 2023, **13**(46), 32083–32096.
76 S. Kim, Y.-S. Yun and Y.-E. Choi, Development of waste biomass based sorbent for removal of cyanotoxin microcystin-LR from aqueous phases, *Bioresour. Technol.*, 2018, **247**, 690–696.
77 S. Ozkan, H. I. Unal, E. Yılmaz and Z. Suludere, Electrokinetic and antibacterial properties of needle like–TiO2/polyrhodanine core/shell hybrid nanostructures, *J. Appl. Polym. Sci.*, 2015, **132**(9). Q15
78 P. Karami, M. M. Haque Mizan, B. Khorshidi, S. Aghapour Aktij, A. Rahimpour, J. Soares, *et al.*, Novel Forward Osmosis Membranes Engineered with Polydopamine/Graphene Oxide Interlayers: Synergistic Impact of Monomer Reactivity and Hydrophilic Interlayers, *Ind. Eng. Chem. Res.*, 2023. Q16 Q17
79 Z. Liu, Z. An, Z. Mi, Z. Wang, Q. Zhu, D. Zhang, *et al.*, Thin-film composite nanofiltration membranes with poly

(amidoxime) as organic interlayer for effective desalination, *J. Environ. Chem. Eng.*, 2022, **10**(1), 107015.
80 W. Li, C. Bian, C. Fu, A. Zhou, C. Shi and J. Zhang, A poly (amide-co-ester) nanofiltration membrane using monomers of glucose and trimesoyl chloride, *J. Membr. Sci.*, 2016, **504**, 185–195.
81 W. Fang, L. Shi and R. Wang, Mixed polyamide-based composite nanofiltration hollow fiber membranes with improved low-pressure water softening capability, *J. Membr. Sci.*, 2014, **468**, 52–61.
82 S. Yu, M. Ma, J. Liu, J. Tao, M. Liu and C. Gao, Study on polyamide thin-film composite nanofiltration membrane by interfacial polymerization of polyvinylamine (PVAm) and isophthaloyl chloride (IPC), *J. Membr. Sci.*, 2011, **379**(1–2), 164–173.
83 M. Zhang, X. You, K. Xiao, Z. Yin, J. Yuan, J. Zhao, *et al.*, Modulating interfacial polymerization with phytate as aqueous-phase additive for highly-permselective nanofiltration membranes, *J. Membr. Sci.*, 2022, **657**, 120673.
84 S. Verissimo, K.-V. Peinemann and J. Bordado, Influence of the diamine structure on the nanofiltration performance, surface morphology and surface charge of the composite polyamide membranes, *J. Membr. Sci.*, 2006, **279**(1–2), 266–275.
85 S. Abu-Obaid, S. A. Aktij, S. Tabe, M. Sadrzadeh and R. R. Farnood, Surfactant-modified adsorptive electrospun nanofiber membrane impregnated with akageneite for phosphorus recovery from wastewater, *J. Environ. Chem. Eng.*, 2022, **10**(6), 108786.
86 A. Asad, S. A. Aktij, P. Karami, D. Sameoto and M. Sadrzadeh, Micropatterned thin-film composite poly (piperazine-amide) nanofiltration membranes for wastewater treatment, *ACS Appl. Polym. Mater.*, 2021, **3**(12), 6653–6665.
87 D. Wu, S. Yu, D. Lawless and X. Feng, Thin film composite nanofiltration membranes fabricated from polymeric amine polyethylenimine imbedded with monomeric amine piperazine for enhanced salt separations, *React. Funct. Polym.*, 2015, **86**, 168–183.
88 L. Shen, W.-s. Hung, J. Zuo, X. Zhang, J.-Y. Lai and Y. Wang, High-performance thin-film composite polyamide membranes developed with green ultrasound-assisted interfacial polymerization, *J. Membr. Sci.*, 2019, **570**, 112–119.
89 J. Luo and Y. Wan, Effects of pH and salt on nanofiltration—a critical review, *J. Membr. Sci.*, 2013, **438**, 18–28.
90 C. Y. Tang, Y.-N. Kwon and J. O. Leckie, Effect of membrane chemistry and coating layer on physiochemical properties of thin film composite polyamide RO and NF membranes: II. Membrane physiochemical properties and their dependence on polyamide and coating layers, *Desalination*, 2009, **242**(1–3), 168–182.
91 W. Zhao, H. Liu, N. Meng, M. Jian, H. Wang and X. Zhang, Graphene oxide incorporated thin film nanocomposite membrane at low concentration monomers, *J. Membr. Sci.*, 2018, **565**, 380–389.
92 M.-X. Pham, T. M. Le, T. T. Tran, H. K. P. Ha, M. T. Phong, V.-H. Nguyen, *et al.*, Fabrication and characterization of polyamide thin-film composite membrane via interfacial polycondensation for pervaporation separation of salt and arsenic from water, *RSC Adv.*, 2021, **11**(63), 39657–39665.
93 M. N. Romanelli, D. Manetti, L. Braconi, S. Dei, A. Gabellini and E. Teodori, The piperazine scaffold for novel drug discovery efforts: the evidence to date, *Expert Opin. Drug Discovery*, 2022, **17**(9), 969–984.
94 D. Keyworth, Ionization Constants for Some Piperazine Derivatives, *J. Org. Chem.*, 1959, **24**(9), 1355–1356.
95 N. J. Salah and B. J. Kadhim, Study of the Cure Reaction of Epoxy Resin Diglycidyl Ether of Bisphenol-A (DGEBA) with Meta-Phenylene Diamine, *Eng. Technol. J., Part A*, 2013, **31**(9). Q18 Q19
96 R. L. Benoit, M. J. Mackinnon and L. Bergeron, Basicity of N-substituted anilines and pyridine in dimethylsulfoxide, *Can. J. Chem.*, 1981, **59**(10), 1501–1504.
97 D. W. Urry, The change in Gibbs free energy for hydrophobic association: Derivation and evaluation by means of inverse temperature transitions, *Chem. Phys. Lett.*, 2004, **399**(1–3), 177–183.
98 E.-A. Zen, Gibbs free energy, enthalpy, and entropy of ten rock-forming minerals: calculations, discrepancies, implications, *Am. Mineral.*, 1972, **57**(3–4_Part_1), 524–553.
99 Z. Tan, S. Chen, X. Peng, L. Zhang and C. Gao, Polyamide membranes with nanoscale Turing structures for water purification, *Science*, 2018, **360**(6388), 518–521.
100 R. Zhang, Q. Sun, J. Tian, B. Van der Bruggen and J. Zhu, Narrowing the pore size distribution of a piperazine-based ultrathin polyamide film with the addition of 1, 3-diamino-2-propanol (DAP), *J. Membr. Sci.*, 2024, 122501.
101 R. N. Wenzel, Surface roughness and contact angle, *J. Phys. Chem.*, 1949, **53**(9), 1466–1467.
102 M. F. Ismail, B. Khorshidi and M. Sadrzadeh, New insights into the impact of nanoscale surface heterogeneity on the wettability of polymeric membranes, *J. Membr. Sci.*, 2019, **590**, 117270.
103 Y. Liang, Y. Zhu, C. Liu, K.-R. Lee, W.-S. Hung, Z. Wang, *et al.*, Polyamide nanofiltration membrane with highly uniform sub-nanometre pores for sub-1 Å precision separation, *Nat. Commun.*, 2020, **11**(1), 2015.
104 W. Xie, G. M. Geise, B. D. Freeman, H.-S. Lee, G. Byun and J. E. McGrath, Polyamide interfacial composite membranes prepared from *m*-phenylene diamine, trimesoyl chloride and a new disulfonated diamine, *J. Membr. Sci.*, 2012, **403**, 152–161.
105 S. Ma, X. Wu, L. Fan, Q. Wang, Y. Hu and Z. Xie, Effect of Different Draw Solutions on Concentration Polarization in a Forward Osmosis Process: Theoretical Modeling and Experimental Validation, *Ind. Eng. Chem. Res.*, 2023, **62**(8), 3672–3683.
106 Y. Zhou, Y. Shi, D. Cai, W. Yan, Y. Zhou and C. Gao, Support-free interfacial polymerized polyamide mem-

 This journal is © The Royal Society of Chemistry 2024

brane on a macroporous substrate to reduce internal concentration polarization and increase water flux in forward osmosis, *J. Membr. Sci.*, 2024, **689**, 122165.
107 A. N. Beni, I. Ghofrani, A. Nouri-Borujerdi, A. Moosavi and D. M. Warsinger, Membrane properties overview in integrated forward osmosis/osmotically assisted reverse osmosis systems, *Desalination*, 2024, **569**, 117008.
108 S. Xu, F. Li, B. Su, M. Z. Hu, X. Gao and C. Gao, Novel graphene quantum dots (GQDs)-incorporated thin film composite (TFC) membranes for forward osmosis (FO) desalination, *Desalination*, 2019, **451**, 219–230.
109 W. A. Phillip, J. S. Yong and M. Elimelech, Reverse draw solute permeation in forward osmosis: modeling and experiments, *Environ. Sci. Technol.*, 2010, **44**(13), 5170–5176.
110 A. P. Straub, A. Deshmukh and M. Elimelech, Pressure-retarded osmosis for power generation from salinity gradients: is it viable?, *Energy Environ. Sci.*, 2016, **9**(1), 31–48.
111 S. E. Skilhagen, Osmotic power—a new, renewable energy source, *Desalin. Water Treat.*, 2010, **15**(1–3), 271–278.
112 S. Chou, R. Wang, L. Shi, Q. She, C. Tang and A. G. Fane, Thin-film composite hollow fiber membranes for pressure retarded osmosis (PRO) process with high power density, *J. Membr. Sci.*, 2012, **389**, 25–33.
113 M. Tian, R. Wang, K. Goh, Y. Liao and A. G. Fane, Synthesis and characterization of high-performance novel thin film nanocomposite PRO membranes with tiered nanofiber support reinforced by functionalized carbon nanotubes, *J. Membr. Sci.*, 2015, **486**, 151–160.
114 Y. Chen, L. Setiawan, S. Chou, X. Hu and R. Wang, Identification of safe and stable operation conditions for pressure retarded osmosis with high performance hollow fiber membrane, *J. Membr. Sci.*, 2016, **503**, 90–100.
115 X. Song, Z. Liu and D. D. Sun, Energy recovery from concentrated seawater brine by thin-film nanofiber composite pressure retarded osmosis membranes with high power density, *Energy Environ. Sci.*, 2013, **6**(4), 1199–1210.
116 M. Dadashi Firouzjaei, A. A. Shamsabadi, A. Rahimpour, F. Akbari Afkhami and M. Elliott, Functionality review and life cycle assessment of a silver-based MOF for advanced material and sustainability applications, *Graphene 2D Nanomater.*, 2024.
117 G. Han, S. Zhang, X. Li and T.-S. Chung, High performance thin film composite pressure retarded osmosis (PRO) membranes for renewable salinity-gradient energy generation, *J. Membr. Sci.*, 2013, **440**, 108–121.
118 Y. Cui, X.-Y. Liu and T.-S. Chung, Enhanced osmotic energy generation from salinity gradients by modifying thin film composite membranes, *Chem. Eng. J.*, 2014, **242**, 195–203.
119 A. Achilli, T. Y. Cath and A. E. Childress, Power generation with pressure retarded osmosis: An experimental and theoretical investigation, *J. Membr. Sci.*, 2009, **343**(1–2), 42–52.
120 S. N. A. Idris and N. Jullok, Evaluation of commercial reverse osmosis and forward osmosis membranes at different draw solution concentration in pressure retarded osmosis process, *Mater. Today: Proc.*, 2021, **46**, 2065–2069.
121 X. Li, T. S. Chung and T. S. Chung, Effects of free volume in thin–film composite membranes on osmotic power generation, *AIChE J.*, 2013, **59**(12), 4749–4761.
122 S. N. A. Idris, N. Jullok, W. J. Lau, A. H. Ma'Radzi, H. L. Ong, M. M. Ramli, *et al.*, Modification of Thin Film Composite Pressure Retarded Osmosis Membrane by Polyethylene Glycol with Different Molecular Weights, *Membranes*, 2022, **12**(3), 282.
123 R. R. Gonzales, M. J. Park, T.-H. Bae, Y. Yang, A. Abdel-Wahab, S. Phuntsho, *et al.*, Melamine-based covalent organic framework-incorporated thin film nanocomposite membrane for enhanced osmotic power generation, *Desalination*, 2019, **459**, 10–19.
124 A. P. Straub, N. Y. Yip and M. Elimelech, Raising the bar: increased hydraulic pressure allows unprecedented high power densities in pressure-retarded osmosis, *Environ. Sci. Technol. Lett.*, 2014, **1**(1), 55–59.
125 S. N. A. Idris, N. Jullok, W. J. Lau, H. L. Ong and C.-D. Dong, Graphene oxide incorporated polysulfone substrate for flat sheet thin film nanocomposite pressure retarded osmosis membrane, *Membranes*, 2020, **10**(12), 416.
126 J. Wei, Y. Li, L. Setiawan and R. Wang, Influence of macromolecular additive on reinforced flat-sheet thin film composite pressure-retarded osmosis membranes, *J. Membr. Sci.*, 2016, **511**, 54–64.
127 X. Wang, S. Gao, J. Wang, S. Xu, H. Li, K. Chen, *et al.*, The production of biobased diamines from renewable carbon sources: Current advances and perspectives, *Chin. J. Chem. Eng.*, 2021, **30**, 4–13.
128 M. F. Shohur, Z. Harun, M. R. Jamalludin, S. K. Hubadillah and M. Z. Yunos, Antifouling and antibacterial study of PSf/bio-ZnO nanoparticle (bio-ZnO NP) mixed matrix membrane for humic acid separation, *Braz. J. Chem. Eng.*, 2024, 1–22.
129 D. S. Rajendran, E. G. Devi, V. Subikshaa, P. Sethi, A. Patil, A. Chakraborty, *et al.*, Recent advances in various cleaning strategies to control membrane fouling: a comprehensive review, *Clean Technol. Environ. Policy*, 2024, 1–16.
130 H. R. Lotfy, J. Staš and H. Roubík, Renewable energy powered membrane desalination—review of recent development, *Environ. Sci. Pollut. Res.*, 2022, **29**(31), 46552–46568.